Two-Stage MPC-Based Energy Optimization Scheduling for a Virtual Power Plant With Multiple Adjustable Resources in Electricity Spot

IET Generation, Transmission & Distribution

WILEY

The Institution of Engineering and Technology

ORIGINAL RESEARCH OPEN ACCESS

Two-Stage MPC-Based Energy Optimization Scheduling for a Virtual Power Plant With Multiple Adjustable Resources in Electricity Spot Markets

Xiang Chen[1] | Jinrui Tang[1,2] | Haochen Li[3] | Changjun Xie[1] | Binyu Xiong[1] | Yang Li[4] | Xinhao Bian[5] | Keliang Zhou[1,2] | Leiming Suo[1] | Jing Wan[6] | Chengqing Yuan[2,5]

[1]School of Automation, Wuhan University of Technology, Wuhan, China | [2]State Key Laboratory of Maritime Technology and Safety, Wuhan University of Technology, Wuhan, China | [3]State Grid Hubeielectric Power Co. Ltd. Ultra High Voltage Company, Wuhan, China | [4]Department of Electrical Engineering, Chalmers University of Technology, Gothenburg, Sweden | [5]School of Transportation and Logistics Engineering, Wuhan University of Technology, Wuhan, China | [6]Economic and Technological Research Institute of State Grid Hubei Electric Power Co., Ltd, Wuhan, China

Correspondence: Jinrui Tang (tangjinrui@whut.edu.cn)

Received: 10 December 2025 | **Revised:** 11 February 2026 | **Accepted:** 13 April 2026

ABSTRACT

To address the reliable and economical operation of virtual power plants containing a large number of adjustable resources in the day-ahead and intraday markets, a two-stage model predictive control (MPC) based optimization scheduling strategies for virtual power plants (VPPs) in the electricity spot market is proposed and discussed in this paper. Firstly, a TCN-GRU-attention hybrid prediction algorithm is developed for forecasting output of inelastic loads, wind power and photovoltaic (PV) in VPPs. Secondly, a hierarchical bi-level mixed-integer linear programming model integrating multiple resources with EV participation is established to enable that EV charging load, GT generation and ESS can dynamically adjust their behaviour under different operation cost. Furthermore, an improved MPC-based intraday dispatch strategy embedded with a bidirectional dynamic penalty mechanism is proposed to rapidly respond to real-time fluctuations of uncontrollable resources. The proposed two-stage MPC-based scheduling strategies can thereby enhance the flexibility and operational efficiency of the VPP system. Simulation results demonstrate that the two-stage collaborative optimization improves the total revenue of VPPs by 5.06%, fully verifying the robust economic advantages of the proposed solution in complex market environments.

1 | Introduction

The energy scheduling methods of traditional power system are focused on the unit commitment, which can reduce the total fuel costs for the unit and avoid power overload in transmission lines [1]. As the development of renewable energy power generation technologies, power systems increasingly incorporate vast numbers of non-dispatchable power sources controlled by converters. This significantly increases the number of variables in power system energy optimization scheduling. Thermal power units face start-stop peak regulation challenges, necessitating the introduction of energy storage systems to fully integrate renewable sources. Consequently, solving optimization problems becomes increasingly difficult in the integrated energy system [2].

Wind and solar energy sources exhibit inherent intermittency and volatility, hence microgrid technologies have been proposed to significantly enhance the self-sustainability of local grid and avoid long-distance transmission of energy [3]. As another typical measure to integrate distributed energy sources (DERs), demand response (DR), energy storage system (ESS), virtual power plant (VPP) has provided an efficient platform to aggregate geographically dispersed adjustable resources through advanced communication technologies and software architectures [4].

VPPs can mitigate adverse grid impacts associated with high penetration of geographical RESs. In the meantime, VPPs can also gain commercial benefits through participating electricity markets like conventional power plants.

In refs. [5, 6], the modeling techniques and energy management methods of VPPs before 2021 have been comprehensively reviewed. In recent years, numerous virtual power plant projects have been put into operation around the world, with an increasing number of aggregated resources, such as electrolytic hydrogen production units, being integrated into these virtual power plants to enhance their flexibility when participating in electricity markets [7–9]. Consequently, recent research has focused on the business models of virtual power plants and optimization scheduling problems under high proportion of renewable energy [10]. In the optimization methods, researchers have paid a great deal of enthusiasm in deep learning-based optimization methods to address the growing complexity of VPP scheduling models [11–13]. Among these literatures, the optimization algorithms and demand response of the aggregated loads have been well studied and the results show that VPPs can significantly enhance the overall efficiency of the system during multi-resource integrated operation.

Nowadays, electricity markets have become a key mechanism for reflecting real-time power supply and demand, with spot prices and medium-to-long-term prices reflecting the actual economic value of flexibly dispatching resources [14]. How to effectively guide the optimized operation of virtual power plants within electricity markets to realize market-based returns on economic value is a problem that should be addressed at present [15]. When participating in the electricity spot market, VPPs must formulate day-ahead trading strategies based on prediction results and must dynamically adjust their scheduling strategies in real time to accommodate discrepancies between actual load and renewable energy output and forecast results in the intraday dispatch [16, 17].

In the day-ahead energy optimization scheduling of VPPs, accurate forecasting of renewable generation and load demand within the VPP is essential to maintain economic viability and ensure power balance. And then these forecast curves are then used to dispatch the adjustable resources in the VPP. These existing optimization methods of VPPs can be mainly divided into stochastic optimization and deterministic optimization methods. Stochastic optimization methods can effectively quantify the randomness of new energy generation and load fluctuations [18, 19]. However, they require dispatchers to possess multi-scenario analysis capabilities when formulating VPP dispatch strategies within electricity markets, which would bring cost risks under extreme scenarios. Hence deterministic optimization methods of VPPs are widely applied in electricity market. Ref. [20] utilized a robust optimization (RO) technique to develop an optimal energy dispatch plan for a VPP engaging in the spot market. This approach takes into consideration all potential uncertainties that may occur during the dispatch process. Nevertheless, robust optimization adopts a worst-case scenario approach, which may lead to overly conservative dispatch plans for VPP, reserving excessive spare capacity or sacrificing economic efficiency to address low-probability extreme events. Ref. [21] adopts the opportunity strategy based on Information gap decision theory (IGDT) to address the uncertainties in VPP operation within electricity markets. By setting a profit growth target, this approach aims to maximize potential returns under minimal uncertainty. However, it fails to balance the trade-off between robustness and opportunity, potentially leading to overly optimistic decisions under high uncertainty. Moreover, its effectiveness heavily relies on the subjectively defined performance target, which, if improperly set, may compromise the strategy's overall performance. Ref. [22] extensively examined the coordination and compatibility of different adjustable resources on the source, grid and load sides. They developed a bi-level optimization energy dispatch model with the objective of minimizing load loss rate, user cost and operational cost, while ensuring a balance between system reliability and economic efficiency. However, this strategy only concentrates on the day-ahead market and faces difficulties in promptly adapting to uncertainties between the power supply and load in the intraday market. This could result in discrepancies between the ideal output of controllable devices and the actual demand for electricity in the intraday market. In the meantime, several deep learning-based methods have been proposed to deal with the day-ahead scheduling for VPPs [23–25]. Reinforcement learning (RL) demonstrates significant potential in dispatch optimization of VPPs in day-ahead spot electricity market. RL-based scheduling algorithms can enable adaptive control and handle complex nonlinear problems. But its practical application faces substantial challenges and limitations. These shortcomings primarily stem from a fundamental conflict between the inherent characteristics of RL algorithms and the rigid scheduling requirements of VPPs. Its core flaw lies in the inability to strictly guarantee compliance with all constraints. In the meantime, RL-based scheduling of VPPs may fail to effectively learn coping strategies due to insufficient training data under low-frequency yet high-risk tail events, such as N−1 faults or extreme weather.

In the intraday energy optimization scheduling of VPPs, stochastic nature of renewable resources induces forecast deviations, potentially reducing VPP's revenue during the intraday stage [26, 27]. To address these challenges, ref. [28] introduced a VPP energy management approach that utilizes model predictive control (MPC) to tackle these problems. This approach employs real-time measurement data to conduct rolling optimization of controllable device output, resulting in a notable improvement in the utilization efficiency of distributed generators. Additionally, it reduces the influence of forecast errors on intraday optimization outcomes when compared to traditional optimization schemes. Nevertheless, this strategy is only suitable for power markets that are regulated by the government. Deregulated energy markets give clients with a greater range of options compared to regulated markets, allowing them to choose services from several electricity providers. This promotes a competitive environment among service providers, leading to a decrease in overall prices [29]. Nevertheless, in markets without regulations, the prices of power are established based on the current supply and demand conditions, leading to substantial fluctuations in pricing and the implementation of more adaptable penalty systems in the intraday stage [30]. This presents more difficulties for implementing MPC in VPP energy dispatch. Ref. [31] enhanced the objective function of MPC and introduced a multi-stage optimal energy management system that is well-suited for deregulated power markets. In addition, Ref. [32] investigated the temporal horizon optimization of MPC in deregulated markets. The study showed that using receding

horizon MPC at the VPP intraday optimization stage leads to greater economic advantages compared to using fixed horizon MPC.

However, in the studies on VPP dispatch methods in the electricity spot market, ESSs are often set as the primary responders to electricity load changes, such as electric vehicles (EV) charging load fluctuation [33, 34]. While this strategy achieves the basic criterion for power balance in the grid, it fails to completely analyse and enhance the entire system performance. With the rapid development of vehicle-to-grid (V2G) technology, the charging load of EVs are rapidly incorporated into the grid architecture, enabling new opportunities for dynamic equilibrium in the power system [35]. In future operation of VPPs, the interaction among these multiple adjustable resources should not be constrained to unidirectional response. Instead, flexible load resources should be able to finely and swiftly change their demand plans based on real-time feedback from the generating schedules of power generation resources. This bidirectional optimization not only boosts the system's responsiveness to renewable energy swings but also encourages the collaborative optimization of source, grid, load and storage resources in electricity spot market [36].

To address the reliable and economical operation of virtual power plants containing a large number of adjustable resources in the day-ahead and intraday markets, this paper delves into the energy optimization scheduling strategies for VPPs with multiple adjustable resources in electricity spot market. The VPP include inelastic loads and flexible EV charging loads in the load side, and uncontrollable WT generators and PV stations in the source-storage side, along with controllable ESS and gas turbine (GT). In both day-ahead and intra-day stages of the electricity spot market, two-stage MPC-based energy optimization scheduling for a VPP with multiple adjustable resources is proposed to ensure system stability and maximizes VPP revenues in the market. The main contributions of this paper are as follows:

- A two-stage MPC optimization scheduling model is proposed for a VPP in both the day-ahead and intraday stages under electricity spot market considering consumers with inelastic demand, adjustable EV charging load, gas turbine generation, wind turbine generation, photovoltaic station and energy storage system.
- Integrated an MPC-based strategy and a bi-level optimization algorithm into the intraday energy management framework to improve VPP operational efficiency under electricity spot market. This enables a rapid response of controllable resources to real-time changes in uncontrollable resources, while allowing EV fleets to dynamically adjust their charging and discharging demands based on real-time feedback from the generation schedules of source-type resources, thereby enhancing flexibility and system adaptability.
- A day-ahead energy management framework incorporates a temporal convolutional network (TCN)-GRU-attention based load forecasting algorithm is proposed to reduce the adverse effects of unpredictable load demand and renewable energy output on the economic efficiency of VPPs under electricity spot market. This approach utilizes the simplicity and efficiency of GRU to decrease computational burden, while the strong feature extraction capability of the and the weighted mechanism of attention improve the accuracy of predicting uncontrollable load demand and new energy output.

The rest of this paper is organized as follows. Section 2 introduces the concept of VPP operation in two-stage electricity spot market. Section 3 provides a detailed illustration of our proposed two-stage MPC-based energy optimization scheduling for a VPP with multiple adjustable resources. Section 4 presents the operation results of a VPP case using field data. Section 5 summarizes the research findings and discusses future prospects.

2 | VPP Operation in Two-Stage Electricity Spot Market With Multiple Adjustable Resources

VPPs aggregate heterogeneous resources, including uncontrollable resources and adjustable resources. The uncontrollable resources include inelastic loads in the load side, and uncontrollable WT and PV units in the source sides. The adjustable resources include EV charging load and controllable ESS and GT generators.

In electricity spot market, market organizers employ security-constrained economic dispatch (SCED) to determine day-ahead clearing prices in the day-ahead market and then inform VPP aggregators. In this paper, VPP aggregators are characterized by their limited scale, which means they have no impact on market prices and do not participate in price rivalry with other VPPs. VPP aggregators, who are involved in the spot market, must complete power dispatch plans the day before the operation day and enter into day-ahead power purchase and sale contracts with network operators. Therefore, there are two stages for VPP operation in electricity spot market, including day-ahead stage and intraday stage.

In order to participate in the spot market, a VPP must formulate binding power purchase and sale strategies with the electricity market based on aggregated internal resource balancing before the actual trading day (denoted as the day-ahead stage). During the intraday stage, unpredictable variations in uncontrollable resources may cause deviations between real-time power transactions and day-ahead scheduled quantities. As a result, the VPP operator may be responsible for paying penalty fees that correspond to these deviations, the penalty price fluctuates based on real-time conditions. The penalty price would be greater than the real-time price for additional purchased electricity or decreased sales electricity than the planned amount in the day-ahead stage, there will be a greater penalty than the real-time price. And the VPP operator will receive a subsidy at a lower rate than the real-time pricing in all other cases in the intraday stage.

As shown in Figure 1a, there are none adjustable resources in the VPP in the two-stage electricity spot market. The planned transaction electricity between the VPP and the power grid is determined by the difference between the predicted uncontrollable load and predicted output power of the PV station and WT generator in the day-ahead stage. In the intraday stage, the actual uncontrollable load and output power of the renewable resources are different from the predicted values. Hence the actual transaction electricity between the VPP and the power grid is different from the planned electricity in the day-ahead stage.

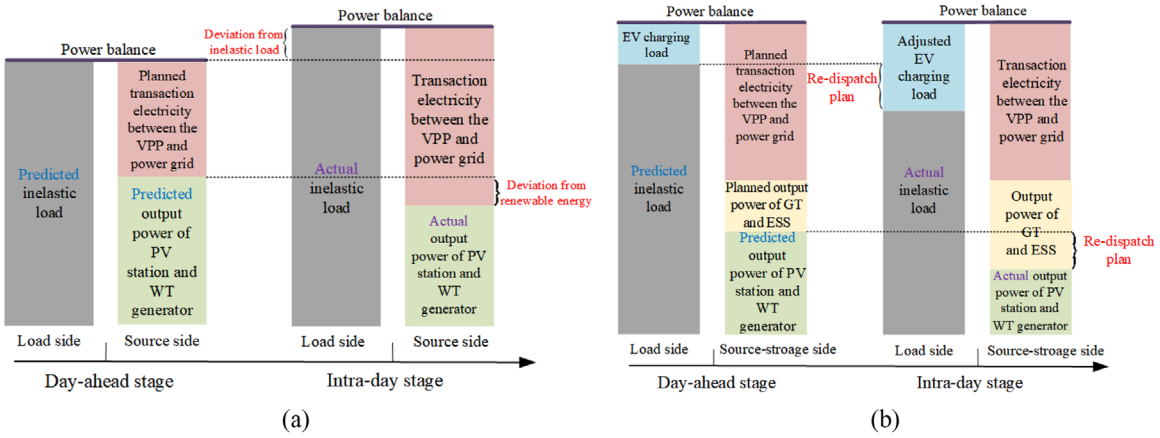

FIGURE 1 | Dispatch scenarios of VPP in two stage electricity market: (a) without controllable resources; (b) integration of controllable resources.

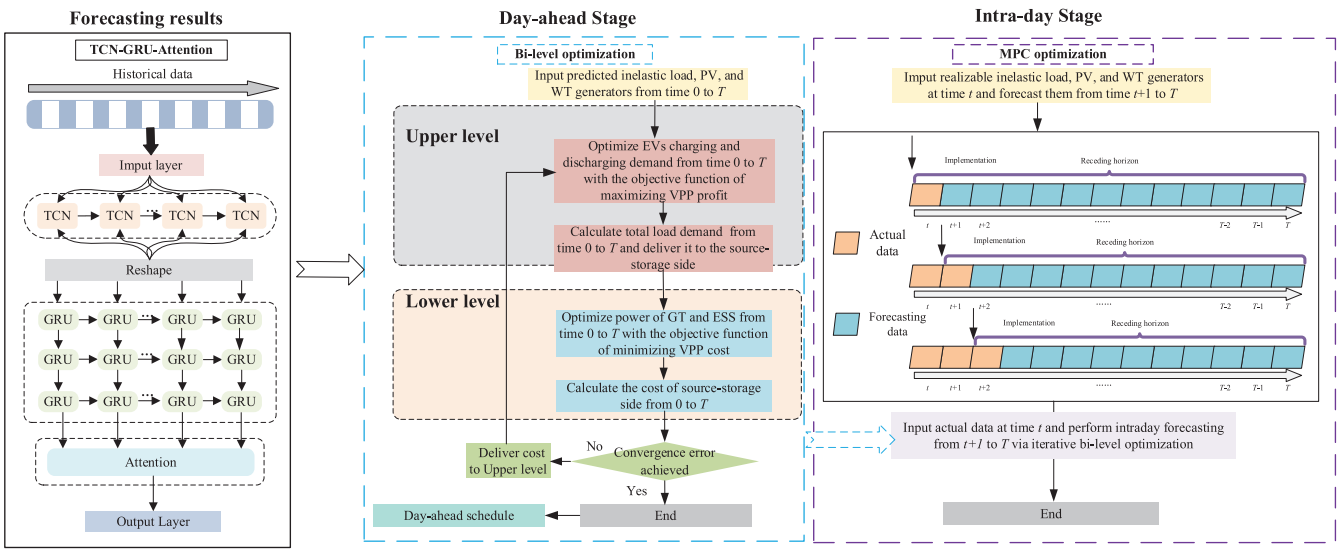

FIGURE 2 | VPP Operation in two-stage electricity spot market with multiple adjustable resources.

Different from Figure 1a, there are multiple adjustable resources in the VPP, including EV charging load and controllable ESS and GT generators, as shown in Figure 1b. In the day-ahead market, the planned output power of ESS and GT generators, and planned transaction electricity between the VPP and power grid would be identified by the economic optimization of the VPP under the constraints of power balance. In the intraday stage, the actual inelastic load and output power of PV station and WT generators differ from the predicted values. Hence the output power of GT and ESS, EV charging load and the transaction electricity are optimized to minimum the total operation cost of the VPP.

3 | Two-Stage MPC-Based Energy Optimization Model for VPP

Figure 2 illustrates the proposed two-stage MPC-based energy optimization model for VPP. The demand response of EV charging loads and the adjustable ESS and GT generation are simultaneously optimized in the spot market. This enables the cooperative optimization of the source, grid, load and storage, hence improving the operational efficiency of the VPP in deregulated spot markets. In order to reduce the effects of uncertainties of inelastic loads and uncontrollable WT and PV units on the VPP operation, the TGA-based forecasting method is used to predict the power of these uncontrollable resources in advance. These predictions establish the day-ahead reference schedule for VPP operations. The MPC approach is utilized in the intraday stage to enable rapid adaptation of adjustable resources to real-time fluctuations in uncontrollable resources. By continuously tracking deviations from the day-ahead schedule curve and implementing rolling adjustments, this method ensures system stability while maximizing economic benefits.

The duration of operating day is represented as T. In the day-ahead stage, the TGA algorithm predicts the inelastic load profiles, input into the day-ahead scheduling model of the VPP load side. Concurrently, forecasted PV and WT generation data is simultaneously fed into the day-ahead scheduling model of the VPP source-storage side. Afterwards, the load side performs the initial round of day-ahead optimization, aiming to maximize the profit that the VPP may achieve in the day-ahead market. This optimization entails modifying the power used for charging and discharging controllable EV units, as well as GT and ESS to

formulate generation plans from time 0 to T and power purchase and sale transaction plans with the grid. This stage aims to maximize the VPP's day-ahead market revenue as the upper-level objective, focusing on reducing GT/ESS operational costs and grid transaction expenses. Increasing the amount of power sold by the load side theoretically results in higher revenue. However, increased load-side sales raise revenue but increase source-storage-side operating costs, reducing overall VPP profit. Hence, the operating costs calculated by the lower-level source-storage side are fed back to the upper-level load side, triggering iterative optimization. The load side re-optimizes scheduling based on updated cost data, while the source-storage side reevaluates the revised costs. This cycle continues until the difference between consecutive costs falls below a convergence threshold. Ultimately, the VPP submits an optimized plan to the electricity market containing time-interval power purchase/sale volumes and equipment dispatch instructions, achieving global equilibrium between economic efficiency and technical constraints.

During the intraday stage, a receding-horizon MPC rolling optimization is implemented. Unlike the open-loop scheduling optimization approach, which generates all optimization results for the time interval from 0 to T in the day-ahead stage, the rolling optimization takes advantage of real-time information provided by VPP operators regarding load and renewable energy output. This method aims to minimize the impact of prediction errors on the optimization results. At the start, at time $t = 0$, real-time measurements are introduced for optimization in each bi-level optimization round from time t to T. Once the intraday bi-level optimization from time t to T approaches convergence error, the current round of bi-level optimization concludes, and the optimization variables at time t are released. Afterwards, the time is retroactively adjusted by one increment, and real-time measurements for the subsequent time increment are incorporated to initiate a fresh cycle of bi-level optimization, resulting in a closed-loop intraday optimization process. The process persists until the optimization variables are issued at time T, thereby finalizing the intraday adjustment plan.

3.1 | Day-Ahead Stage

The VPP devises its day-ahead strategy using the day-ahead predictions of uncontrollable resources, including inelastic loads and adaptable EV fleets in the load side, and uncontrollable WT and PV units, as well as controllable ESS and GT in the source-storage side. In order to optimize profits in the spot market while maintaining a balance between power supply and demand, the coordination and synergy of different aggregated resources should be enhanced in the VPP. Therefore, a mixed-integer linear programming (MILP) approach is used to efficiently allocate resources in the operations of controlled and uncontrollable resources on both the load side and the source-storage side. Furthermore, a bi-level optimization algorithm is implemented to enable the VPP to adapt its internal supply-demand dynamics and preserve power equilibrium. This allows the VPP to maximize its profitability in the spot market. The main objective is to concentrate on the scheduling of active power in the VPP, while disregarding reactive power and losses in transmission lines.

(1) **Objective function in the upper level**

The primary goal of the VPP in the day-ahead stage is to optimize the revenue generated from the sale of electricity, and is comprised of two components: the revenue derived from fulfilling the energy needs of inelastic load, and the revenue derived from meeting the charging requirements of EVs for the users. In addition, the VPP offers specific subsidies for the act of discharging users' EVs. Hence the objective function is given by

$$\max \text{profit}_{\text{day-ahead}} = \text{profit}^{\text{Load}}_{\text{day-ahead}} + \text{profit}^{\text{EV}}_{\text{day-ahead}} - \text{cost}_{\text{day-ahead}} \tag{1}$$

$$\text{profit}^{\text{Load}}_{\text{day-ahead}} = \sum_{t=0}^{T} I^{im}_{\text{forcast}}(t) * \alpha_{\text{sell}} * \text{RTP}(t) * \Delta t \tag{2}$$

$$\text{profit}^{\text{EV}}_{\text{day-ahead}} = \sum_{t=0}^{T} \sum_{i=1}^{z} \left(P^{\text{ch,EV}}_{\text{day-ahead},i}(t) * \alpha_{\text{sell}} * \text{RTP}(t) - P^{\text{dis,EV}}_{\text{day-ahead},i}(t) * \delta_{\text{ev}} \right) * \Delta t \tag{3}$$

In the objective function, the discharging or charging power of ith EV, including $P^{\text{dis,EV}}_{\text{day-ahead},i}(t)$ and $P^{\text{ch,EV}}_{\text{day-ahead},i}(t)$, as well as $P^{\text{buy}}_{\text{day-ahead}}(t)$, $P^{\text{sell}}_{\text{day-ahead}}(t)$, $P^{\text{GT}}_{\text{day-ahead}}(t)$, $P^{\text{ch,ESS}}_{\text{day-ahead}}(t)$, $P^{dis,ESS}_{day-ahead}(t)$ are the variables. And the variables $P^{dis,EV}_{day-ahead,i}(t)$ and $P^{ch,EV}_{day-ahead,i}(t)$ are determined by the upper level, which would be further used as the constraints in the lower level.

In the deregulated market, electricity prices are determined by real-time supply and demand relationships. This study does not consider price uncertainty. In Equation (1), z represents the total number of EVs, and the sale price for inelastic load and the charging price for EVs are uniformly expressed as the real-time sale price. The real-time selling price is calculated by multiplying the RTP(t) with the selling price coefficient a_{sell}. The VPP operator offers EV customers a constant subsidy coefficient, denoted as δ_{EV}, The upper-level optimization variables are the $P^{\text{ch,EV}}_{\text{day-ahead},i}(t)$ and $P^{\text{dis,EV}}_{\text{day-ahead},i}(t)$. After completing the upper-level optimization, the total load demand $L_{\text{day-ahead}}(t)$ is calculated and transmitted to the lower-level optimization model.

(2) **Constraints in the upper level**

The upper-level constraints mainly pertain to the EVs within the VPP, with energy and SOC constraints as defined in Equations (4–9).

$$0 \le P^{\text{ch,EV}}_{\text{day-ahead},i}(t) \le P^{\text{ch,EV}}_{i,\max} \tag{4}$$

$$0 \le P^{\text{dis,EV}}_{\text{day-ahead},i}(t) \le P^{\text{dis,EV}}_{i,\max} \tag{5}$$

$$U^{\text{ch,EV}}_{i}(t) + U^{\text{dis,EV}}_{i}(t) = U^{\text{EV}}_{i}(t) \tag{6}$$

$$\text{capicity}^{\text{EV}}_{i} * \left(\text{SoC}^{\text{EV}}_{\text{day-ahead},i}(t) - \text{SoC}^{\text{EV}}_{\text{day-ahead},i}(t-1) \right) = \frac{96}{T} * \left(P^{\text{ch,EV}}_{\text{day-ahead},i}(t) * y^{\text{EV}}_{i} - \frac{P^{\text{dis,EV}}_{\text{day-ahead},i}(t)}{y^{\text{EV}}_{i}} \right) - E^{\text{EV}}_{i} * d^{\text{EV}}_{i}(t) \tag{7}$$

$$\mathrm{SoC}^{\mathrm{EV}}_{\min,i} \le \mathrm{SoC}^{\mathrm{EV}}_{\mathrm{day-ahead},i}(t) \le \mathrm{SoC}^{\mathrm{EV}}_{\max,i} \tag{8}$$

$$\mathrm{SoC}^{\mathrm{EV}}_{i}(1) = \mathrm{SoC}^{\mathrm{EV}}_{i}(T) \tag{9}$$

In Equation (6), the variable $U_i(t)$ denotes the instantaneous condition of ith EV at time t, signifying that an EV can solely charge or discharge when $U_i^{\mathrm{EV}}(t)$ is equal to 1, indicating its connection to the grid. Simultaneous charging and discharging are not possible for the same EV. In Equation (7), the variable E_i^{ev} denotes the power consumption per kilometre for the ith EV, while d_i^{EV} indicates the distance travelled by the ith EV during the time period $[0, t]$ [4].

In Equation (10), $L^{im}_{\mathrm{forecast}}(t)$ denotes the inelastic demand predicted by our proposed algorithm at time t, which would be illustrated in Section 3.3; $L_{\mathrm{day-ahead}}(t)$ represents the total load after day-ahead optimization at time t and will be sent to the optimal model in the lower level to meet the power balance constraints of the lower level. After obtaining the optimal $P^{\mathrm{ch,EV}}_{\mathrm{day-ahead},i}(t)$ and $P^{\mathrm{dis,EV}}_{\mathrm{day-ahead},i}(t)$, the $L_{\mathrm{day-ahead}}(t)$ is calculated and transmitted to the lower-level model.

$$L_{\mathrm{day-ahead}}(t) = L^{im}_{\mathrm{forecast}}(t) + \sum_{i=1}^{z} P^{\mathrm{ch,EV}}_{\mathrm{day-ahead},i}(t) - \sum_{i=1}^{z} P^{\mathrm{dis,EV}}_{\mathrm{day-ahead},i}(t) \tag{10}$$

(3) Objective function in the lower level

The goal of the lower level is to optimize the utilization of different generation and storage resources, minimize operational expenses and satisfy the load demand. This study examines the operational costs of the VPP in the day-ahead stage, which consist of three components: the expenses associated with engaging in the electrical market to purchase and sell power, the costs related to the GT's generation and the expenses linked to the ESS. The lower-level optimization variables include $P^{\mathrm{buy}}_{\mathrm{day-ahead}}(t)$, $P^{\mathrm{sell}}_{\mathrm{day-ahead}}(t)$, $P^{\mathrm{dis,ESS}}_{\mathrm{day-ahead}}(t)$, $P^{\mathrm{ch,ESS}}_{\mathrm{day-ahead}}(t)$ and $P^{\mathrm{GT}}_{\mathrm{day-ahead}}(t)$. After completing the optimization of the lower-level model, the $\cos\mathrm{t}_{\mathrm{day-ahead}}$ is calculated and fed back to the upper-level model.

$$\min \mathrm{cost}_{\mathrm{day-ahead}} = \mathrm{cost}^{\mathrm{Grid}}_{\mathrm{day-ahead}} + \mathrm{cost}^{\mathrm{GT}}_{\mathrm{day-ahead}} + \mathrm{cost}^{\mathrm{ESS}}_{\mathrm{day-ahead}} \tag{11}$$

$$\mathrm{cost}^{\mathrm{Grid}}_{\mathrm{day-ahead}} = \sum_{t=0}^{T} \left(P^{\mathrm{buy}}_{\mathrm{day-ahead}}(t) * \alpha_{\mathrm{buy}} - P^{\mathrm{sell}}_{\mathrm{day-ahead}}(t) * \alpha_{\mathrm{sell}} \right) * \Delta t * \mathrm{RTP}(t) \tag{12}$$

$$\mathrm{cost}^{\mathrm{GT}}_{\mathrm{day-ahead}} = \sum_{t=0}^{T} P^{\mathrm{GT}}_{\mathrm{day-ahead}}(t) * \lambda_{\mathrm{GT}} * \Delta t \tag{13}$$

$$\mathrm{cost}^{\mathrm{ESS}}_{\mathrm{day-ahead}} = \sum_{t=0}^{T} \left(P^{\mathrm{ch,ESS}}_{\mathrm{day-ahead}}(t) + P^{\mathrm{dis,ESS}}_{\mathrm{day-ahead}}(t) \right) * \lambda_{\mathrm{ESS}} * \Delta t \tag{14}$$

In Equation (11), $\mathrm{cost}^{\mathrm{Grid}}_{\mathrm{day-ahead}}$ denotes the electricity purchasing and selling cost of the VPP when participating in the electricity market during the day-ahead stage.$\mathrm{cost}^{\mathrm{GT}}_{\mathrm{day-ahead}}$ represents the power generation cost of the GT within the VPP in the day-ahead stage, while $\mathrm{cost}^{\mathrm{ESS}}_{\mathrm{day-ahead}}$ stands for the operation cost of the ESS in the VPP during this stage. Furthermore, in Equation (10), $P^{\mathrm{buy}}_{\mathrm{day-ahead}}(t)$ and $P^{\mathrm{sell}}_{\mathrm{day-ahead}}(t)$ refer to the electricity purchasing power and selling power of the VPP at time t in the day-ahead stage, respectively.

In the electricity spot market, the VPP operator is required to remit a transmission fee to the grid when selling electricity. Consequently, the current purchase price is greater than the current selling price and is calculated by multiplying RTP(t) by the purchase price coefficient α_{buy}.

In Equation (13), $P^{\mathrm{GT}}_{\mathrm{day-ahead}}(t)$ is the power generation power of the GT at time t in the day-ahead stage, and λ_{GT} is the operation cost coefficient of the GT. In Equation (14), $P^{\mathrm{ch,ESS}}_{\mathrm{day-ahead}}(t)$ and $P^{\mathrm{dis,ESS}}_{\mathrm{day-ahead}}(t)$ are the charging and discharging powers of the ESS at time t in the day-ahead stage, respectively, and λ_{ESS} is the operation cost coefficient of the ESS. Following the completion of day-ahead optimization, the lower-level model allocates the day-ahead operational costs $\mathrm{cost}_{\mathrm{day-ahead}}$ to the upper level.

(4) Constraints in the lower level

The proposed day-ahead scheduling model requires the lower level to adhere to power balance constraints, ESS constraints, GT limitations and constraints associated with electricity market transactions. Equations (15–28) represent these limitations.

$$P^{\mathrm{buy}}_{\mathrm{day-ahead}}(t) + P^{\mathrm{dis,ESS}}_{\mathrm{day-ahead}}(t) + P^{\mathrm{WT}}_{\mathrm{forecast}}(t) + P^{\mathrm{PV}}_{\mathrm{forecast}}(t) + P^{\mathrm{GT}}_{\mathrm{day-ahead}}(t) = L_{\mathrm{day-ahead}}(t) + P^{\mathrm{sell}}_{\mathrm{day-ahead}}(t) + P^{\mathrm{ch,ESS}}_{\mathrm{day-ahead}}(t) \tag{15}$$

where $L_{\mathrm{day-ahead}}(t)$ denotes the optimized total load for the day-ahead stage on the upper level, whereas $P^{\mathrm{WT}}_{\mathrm{forecast}}$ and $P^{\mathrm{PV}}_{\mathrm{forecast}}$ represent the predicted WT generation and PV station for the day-ahead stage, respectively, generated by the deep learning system.

$$0 \le P^{\mathrm{ch,ESS}}_{\mathrm{day-ahead}}(t) \le P^{\mathrm{ch,ESS}}_{\max} \tag{16}$$

$$0 \le P^{\mathrm{dis,ESS}}_{\mathrm{day-ahead}}(t) \le P^{\mathrm{dis,ESS}}_{\max} \tag{17}$$

$$P^{\mathrm{ch,ESS}}_{\mathrm{day-ahead}}(t) * P^{\mathrm{dis,ESS}}_{\mathrm{day-ahead}}(t) = 0 \tag{18}$$

$$\mathrm{capicity}^{\mathrm{ESS}} * \left(\mathrm{SoC}^{\mathrm{ESS}}_{\mathrm{day-ahead}}(t) - \mathrm{SoC}^{\mathrm{ESS}}_{\mathrm{day-ahead}}(t-1) \right) = \frac{96}{T} * \left(P^{\mathrm{ch,ESS}}_{\mathrm{day-ahead}}(t) * y^{\mathrm{ESS}} - \frac{P^{\mathrm{dis,ESS}}_{\mathrm{day-ahead}}(t)}{y^{\mathrm{ESS}}} \right) \tag{19}$$

$$\mathrm{SoC}^{\mathrm{ESS}}_{\min} \le \mathrm{SoC}^{\mathrm{ESS}}_{\mathrm{day-ahead}}(t) \le \mathrm{SoC}^{\mathrm{ESS}}_{\max} \tag{20}$$

$$\mathrm{SoC}^{\mathrm{ESS}}(1) = \mathrm{SoC}^{\mathrm{ESS}}(T) \tag{21}$$

Equations (16) and (17) correspond to the charge-discharge power constraints of ESS: $P^{\mathrm{ch,ESS}}_{\max}$ denotes the maximum charging power of the ESS, while $P^{\mathrm{dis,ESS}}_{\max}$ represents the maximum discharging power of the ESS. Equation (18) is the operation state constraint of the ESS, which indicates that the ESS cannot perform charging and discharging operations simultaneously. Equation (19) refers to the SOC constraint of the ESS: $\mathrm{capicity}^{\mathrm{ESS}}$ stands for the rated capacity of the ESS, $\mathrm{SOC}^{\mathrm{ESS}}_{\mathrm{day-ahead}}(t)$ denotes the SOC of the

ESS at time t in the day-ahead stage, and y^{ESS} is the charge-discharge efficiency of the ESS. $\mathrm{SOC}^{\mathrm{ESS}}_{\min}$ and $\mathrm{SOC}^{\mathrm{ESS}}_{\max}$ are the SOC upper bound and SOC lower bound of the ESS, respectively. Equation (21) represents the SOC conservation constraint of the ESS.

In this scenario, the limitations of the ESS are analogous to the limitations for the charging and discharging of EVs. ESS has the ability to engage in VPP operational scheduling at any given moment and do not experience any power losses except during the process of charging and discharging.

$$0 \le P^{\mathrm{GT}}_{\mathrm{day-ahead}} \le P^{\mathrm{GT}}_{\max} \tag{22}$$

$$R^{\mathrm{GT}}_{\mathrm{down}} \le P^{\mathrm{GT}}_{\mathrm{day-ahead}}(t) - P^{\mathrm{GT}}_{\mathrm{day-ahead}}(t-1) \le R^{\mathrm{GT}}_{\mathrm{up}} \tag{23}$$

GT is subject to constraints that primarily involve upper and lower limits on output, as well as limitations on the rates at which it can increase or decrease its output.

$$0 \le P^{\mathrm{buy}}_{\mathrm{day-ahead}}(t) \le P^{\mathrm{buy}}_{\max} \tag{24}$$

$$0 \le P^{\mathrm{sell}}_{\mathrm{day-ahead}}(t) \le P^{\mathrm{sell}}_{\max} \tag{25}$$

$$P^{\mathrm{sell}}_{\mathrm{day-ahead}}(t) * P^{\mathrm{buy}}_{\mathrm{day-ahead}}(t) = 0 \tag{26}$$

$$P^{\mathrm{buy}}_{\mathrm{day-ahead}}(t) > 0, P^{\mathrm{grid}}_{\mathrm{day-ahead}}(t) = P^{\mathrm{buy}}_{\mathrm{day-ahead}}(t) \tag{27}$$

$$P^{\mathrm{buy}}_{\mathrm{day-ahead}}(t) \le 0, P^{\mathrm{grid}}_{\mathrm{day-ahead}}(t) = -P^{\mathrm{sell}}_{\mathrm{day-ahead}}(t) \tag{28}$$

The constraints for transactions between the source-storage side of the VPP and the electricity market apply to the electricity purchasing and selling powers. In Equation (24) and Equation (25), $P^{\mathrm{buy}}_{\max}$ and $P^{\mathrm{sell}}_{\max}$ denote the maximum electricity purchasing power and maximum electricity selling power of the VPP, respectively. Equation (26) enforces the mutual exclusion constraint of electricity purchasing and selling operations—meaning these two operations cannot occur concurrently within the same time interval. Equation (27) indicates that the tie-line power of the VPP at time t in the day-ahead stage corresponds to its electricity purchasing power. Equation (28) states that the tie-line power of the VPP at time t in the day-ahead stage corresponds to its electricity selling power.

The termination criterion for the bi-level optimization is the convergence error between two consecutive optimization solutions falling inside the specified range ε. The convergence condition is denoted by Equation (29).

$$\sum_{t=0}^{T} \left| \frac{L^{n+1}_{\mathrm{day-ahead}}(t) - L^{n}_{\mathrm{day-ahead}}(t)}{L^{n}_{\mathrm{day-ahead}}(t)} \right| + \left| \frac{\cos t^{n+1}_{\mathrm{day-ahead}} - \cos t^{n}_{\mathrm{day-ahead}}}{\cos t^{n}_{\mathrm{day-ahead}}} \right| \le \varepsilon \tag{29}$$

In Equation (29), $L^{n+1}_{\mathrm{day-ahead}}(t)$ and $L^{n}_{\mathrm{day-ahead}}(t)$ denote the total load at time t on the load side in the $(n+1)$ th and nth rounds of day-ahead scheduling, respectively. Symbols $\cos t^{n+1}_{\mathrm{day-ahead}}$ and $\cos t^{n}_{\mathrm{day-ahead}}$ refer to the total power generation cost at time t on the source-storage side in the $(n+1)$ th and nth rounds of day-ahead scheduling, respectively.

3.2 | Intra-Day Stage

This study utilizes a MPC-based scheduling optimization method to effectively manage the unpredictable changes in load demand and renewable energy generation in real-time during the intraday period of the deregulated spot market. The main objective is to maximize the profits of the VPP operator during intra-day stage. MPC utilizes the real-time measurements and very short-term predictions for future time intervals to determine a sequence of optimal control decision variables within the optimization period. These variables are determined based on the constraints and objective function. As the sampling and optimization processes continue, the system consistently updates its measurements and conducts ongoing optimization using the previously outlined approach until the specified terminal time is attained [37]. A MPC strategy that leverages a receding horizon mechanism is used in this paper. Optimization is conducted iteratively in this method, commencing at time t and persisting until time T. During each optimization phase, the inelastic demand, PV station and WT generation at time t are regarded as the actual values, while the remaining time periods are treated as forecast values.

In order to allow the EVs in the VPP to adapt their charging and discharging needs according to real-time information, a bi-level optimization is also performed between the upper level and the lower level inside each optimization horizon using the MPC framework. Once the bi-level optimization process is complete, the optimized variables for time t are produced. Subsequently, time t is incremented, initiating the subsequent iteration of intraday optimization. This process persists until the designated terminal time T is attained. The goal function and constraints for the intra-day stage are as follows

(1) Objective function in the upper level

The objective function for the upper-level model in the intra-day stage is the same as in the day-ahead stage with different time scales. The profit comprises the revenue generated from inelastic demand and the revenue generated from the charging and discharging of EVs.

$$\max \mathrm{profit}_{\mathrm{intra-day}} = \mathrm{profit}^{\mathrm{Load}}_{\mathrm{intra-day}} + \mathrm{profit}^{\mathrm{EV}}_{\mathrm{intra-day}} - \mathrm{cost}_{\mathrm{intra-day}} \tag{30}$$

$$\mathrm{profit}^{\mathrm{Load}}_{\mathrm{intra-day}} = \sum_{t}^{T} L^{im}(t) * \alpha_{\mathrm{sell}} * \mathrm{RTP}(t) * \Delta t \tag{31}$$

$$\mathrm{profit}^{\mathrm{EV}}_{\mathrm{intra-day}} = \sum_{t}^{T} \sum_{i=1}^{z} \left(P^{\mathrm{ch,EV}}_{\mathrm{intra-day},i}(t) * \alpha_{\mathrm{sell}} * RTP(t) - P^{\mathrm{dis,EV}}_{\mathrm{intra-day},i}(t) * \delta_{\mathrm{EV}} \right) * \Delta t \tag{32}$$

In Equation (30), $\mathrm{profit}_{\mathrm{intra-day}}$ denotes the total intra-day revenue of the VPP on the load side. $\mathrm{profit}^{\mathrm{Load}}_{\mathrm{intra-day}}$ refers to the intra-day electricity selling revenue of the rigid load on the load side, $\mathrm{profit}^{\mathrm{EV}}_{\mathrm{intra-day}}$ represents the intra-day charge–discharge revenue of EVs on the load side, and $\mathrm{cost}_{\mathrm{intra-day}}$ is the intra-day power generation cost of the source-storage side.

Furthermore, in Equation (31), $L^{im}(t)$ is the load demand of the rigid load at time t in the intra-day stage. Its electricity selling price and EV charging price are uniformly defined as the real-time electricity selling price, which is derived by multiplying the real-time price RTP(t) by the electricity selling price coefficient α_{sell}.

In Equation (32), the intra-day charge-discharge revenue of EVs equals the intra-day charging revenue minus the intra-day discharging subsidy. $P^{\text{ch,EV}}_{\text{intra-day},i}(t)$ denotes the charging power of the ith EV at time t in the intra-day stage, and $P^{\text{dis,EV}}_{\text{intra-day},i}(t)$ represents the discharging power of the ith EV at time t in the intra-day stage.

The operation cost $\text{cost}_{\text{intra-day}}$ of the VPP from time t to T in the intra-day stage is transmitted to the load side after optimization scheduling by the intra-day scheduling model of the source-storage side. In the first iteration of the intra-day bi-level optimization, $\text{cost}_{\text{intra-day}}$ refers to the intra-day operation cost estimated from the historical intra-day optimization of the VPP.

(2) Constraints in the upper level

The power balancing constraint and the energy and SoC limitations for EVs on the upper level in the proposed intraday scheduling model are analogous to those in the day-ahead stage. This research presupposes that the driving distance for EVs remains unaltered during the intra-day stage. The distinction lies in the fact that L^{im} during each cycle of intraday optimization on the upper level corresponds to the actual value at time t within the specified time window, whilst the remaining time periods are considered as predicted values. The energy and SOC limitations for EVs are identical to Equations (2–7). Equation (33) represents the power balance restriction.

$$L_{\text{intra-day}}(t) = L^{im}(t) + \sum_{i=1}^{z} P^{\text{ch,EV}}_{\text{intra-day},i}(t) - \sum_{i=1}^{z} P^{\text{dis,EV}}_{\text{intra-day},i}(t) \quad (33)$$

In Equation (33), the variable $L_{\text{intra-day}}(t)$ represents the total load after the intraday optimization process at time t. Once a round of intraday optimization is completed on the upper level, the value of $L_{\text{intra-day}}(t)$ from time t to T inside that optimization round is transferred to the lower-level model.

(3) Objective function in the lower level

In the intraday stage, the operating expenses of the VPP consist of the GT's generation expenses, the ESS's operational expenses, and the penalties incurred by the VPP for participating in the intraday balancing market, as specified in Equations (34)-(38).

$$\min \text{cost}_{\text{intra-day}} = \text{cost}^{\text{Grid}}_{\text{intra-day}} + \text{cost}^{\text{GT}}_{\text{intra-day}} + \text{cost}^{\text{ESS}}_{\text{intra-day}} \quad (34)$$

$$\text{cost}^{\text{Grid}}_{\text{intra-day}} = \sum_{t}^{T} \Delta P^{\text{Grid}}_{i}(t) * M_i(t) * \Delta t \quad (35)$$

$$\text{cost}^{\text{Grid}}_{\text{intra-day}} = \sum_{t}^{T} \Delta P^{\text{Grid}}_{i}(t) * M_i(t) * \Delta t \quad (36)$$

$$\text{cost}^{\text{ESS}}_{\text{intra-day}} = \sum_{t}^{T} \left(P^{\text{ch,ESS}}_{\text{intra-day}}(t) + P^{\text{dis,ESS}}_{\text{intra-day}}(t) \right) * l_{\text{ESS}} * Dt \quad (37)$$

$$\Delta P^{\text{grid}}_{1}(t) = P^{\text{grid}}_{\text{day-ahead}}(t) - P^{\text{grid}}_{\text{intra-day}}(t) \geq 0 \quad (38)$$

$$\Delta P^{\text{grid}}_{2}(t) = P^{\text{grid}}_{\text{day-ahead}}(t) - P^{\text{grid}}_{\text{intra-day}}(t) < 0 \quad (39)$$

$$M_1(t) = \beta_{\text{punish}} * \text{RTP}(t) \quad (40)$$

$$M_2(t) = \beta_{\text{subsidy}} * \text{RTP}(t) \quad (41)$$

In Equation (34), $\text{cost}^{\text{Grid}}_{\text{intra-day}}$ denotes the penalty incurred by the VPP in the intra-day balancing market, $\text{cost}^{\text{GT}}_{\text{intra-day}}$ represents the power generation cost of the GT within the VPP in the intra-day stage and $\text{cost}^{\text{ESS}}_{\text{intra-day}}$ refers to the operation cost of the ESS in the VPP during this stage.

Since the day-ahead forecasting results of renewable energy output and load demand do not precisely match the actual conditions in the intraday phase, the deregulated market imposes penalties for deviations from the day-ahead purchase or sale plans. Specifically, if the intraday purchased electricity exceeds the day-ahead plan or the sales electricity is lower than the day-ahead plan at time t, the market applies a penalty price higher than the real-time price, denoted as $M_1(t)$, and β_{punish} is the penalty coefficient. Conversely, if the intraday purchased electricity is less than or the sales electricity exceeds the day-ahead plan, a subsidy price lower than the real-time price is provided at time t, denoted as $M_2(t)$ and β_{subsidy} is the subsidy coefficient.

$P^{\text{GT}}_{\text{intra-day}}(t)$ is the power generation power of the GT at time t in the intra-day stage. In Equation (36), $P^{\text{ch,ESS}}_{\text{intra-day}}(t)$ and $P^{\text{dis,ESS}}_{\text{intra-day}}(t)$ denote the charging power and discharging power of the ESS at time t in the intra-day stage, respectively, and λ_{ESS} is the operation cost coefficient of the ESS. After completing a round of day-ahead scheduling, the source-storage side model transmits the day-ahead operation cost $\text{cost}_{\text{intra-day}}$ to the load side.

(4) Constraints in the lower level

Similarly, restrictions such as power balancing, ESS, exist in intraday electricity market transactions in lower-level model.

$$P^{\text{PV}}(t) + P^{\text{dis,ESS}}_{\text{intra-day}}(t) + P^{\text{WT}}(t) + P^{\text{grid}}_{\text{intra-day}}(t) + P^{\text{GT}}_{\text{intra-day}}(t) = L_{\text{intra-day}}(t) + P^{\text{ch,ESS}}_{\text{intra-day}}(t) \quad (42)$$

In Equation (42), $P^{\text{PV}}(t)$ is defined as the intraday solar power generation and $P^{\text{WT}}(t)$ is defined as the intraday wind power generation at time t. During each cycle of intraday optimization at the lower level, they are the real-time monitored values at time t and the predicted values for other time periods within the optimization time range. $L_{\text{intra-day}}(t)$ refers to the total load in intraday optimization on the upper level at time t. The remaining restrictions are identical to Equations (16–28), except that the subscript has been changed to intra-day.

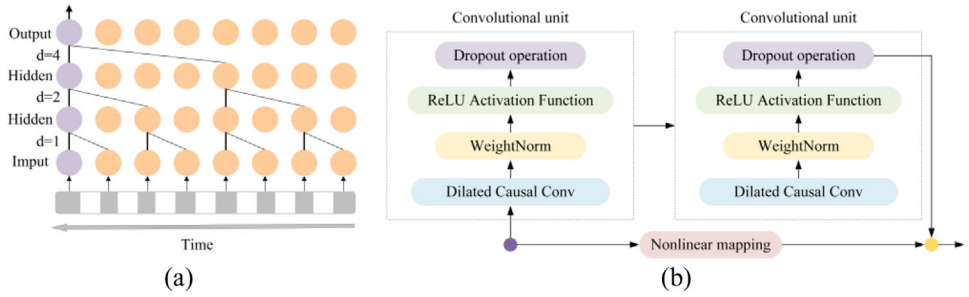

FIGURE 3 | Neural network structure diagram (a) TCN; (b) residual block.

The optimization results fall inside the time range from t to T, just as the convergence conditions of the day-ahead double-layer optimization.

$$\sum_{t}^{T}\left|\frac{L_{\text{intra-day}}^{n+1}(t)-L_{\text{intra-day}}^{n}(t)}{L_{\text{intra-day}}^{n}(t)}\right|+\left|\frac{\text{cost}_{\text{intra-day}}^{n+1}-\text{cost}_{\text{intra-day}}^{n}}{\text{cost}_{\text{intra-day}}^{n}}\right|\leq\varepsilon \tag{43}$$

where $L_{\text{inttra-day}}^{n+1}(t)$ and $L_{\text{intra-day}}^{n}(t)$ denote the intra-day total load at time t on the load side in the $(n+1)$ th and nth rounds of intra-day optimization, respectively.$\text{cost}_{\text{intra-day}}^{n+1}$ and $\text{cost}_{\text{intra-day}}^{n}$ refer to the total operation cost at time t on the source-storage side in the $(n+1)$ th and nth rounds of intra-day optimization, respectively.

3.3 | Day-Ahead Power Forecasting Algorithm

In the two-stage optimization process, in addition to the aforementioned variable coupling, the connection between the two stages also relies on renewable energy output and electricity load forecasting results. As a critical element, forecasting serves as the link between the day-ahead and intra-day stages, directly impacting the effectiveness of the proposed two-stage MPC-based method. If the accuracy of forecasting for inelastic demand and renewable energy output is high, it provides reliable input for the two-stage optimization, ensuring the overall system's operational performance and economic efficiency. However, if the forecasting results show significant deviations, the optimization results may diverge from actual needs, affecting the scheduling efficiency of resources such as EVs and ESS, thereby increasing operational costs. It not only influences day-ahead optimization decisions but also negatively impacts intra-day scheduling, weakening the overall optimization performance.

Different from the load forecasting in traditional power system [38], Forecasting accuracy under different scenarios with high volatility and strong randomness in a small-scale VPP are extremely important for the real-time optimized operation in the spot market. Ref. [39] utilized the backpropagation (BP) artificial neural network to implement VPP energy management for predicting wind power output in Texas. They also suggested techniques to minimize penalty costs resulting from forecast deviations of uncontrollable power sources. However, this study largely concentrated on the ambiguity around emerging energy outputs, disregarding the uncertainty related to load. Ref. [40] took into account the uncertainty of both load and new energy output by using a bi-directional long short-term memory (BiLSTM) forecasting model in the suggested day-ahead energy management framework for VPP. Nevertheless, the time-sensitive nature of the spot market may be hindered by the intricate design of LSTM, leading to a higher computing burden and ultimately restricting its practical use. The gated recurrent unit (GRU) is a simplified version of the LSTM that nevertheless has limitations in capturing local aspects of time series [41, 42]. Thus, it is imperative to implement more effective and dependable forecasting models in VPP.

(1) TCN

During the day-ahead prediction stage, the TCN layer is able to extract relevant information from the load and renewable energy output. This information is then passed on to the neural network model for further learning and propagation. As a result, the neural network model becomes better equipped to capture local features in day-ahead prediction. The structural diagram is depicted in Figure 3a,b. Equation (44) provides the formula for one-dimensional dilated causal convolution, denoted as F(s).

$$F(s)=(x\odot f)(s)=\sum_{i=0}^{k-1}f(i)x_{s-di} \tag{44}$$

The variable k signifies the size of the convolutional kernel, d represents the dilation factor, $s-di$ represents the sequence corresponding to the elements in the convolutional kernel, and $\odot$ represents the convolution operator. The picture displays the structure diagram of the residual block. In this diagram, the TCN input data travels through two iterations of unfolded causal convolution, weight normalization, activation function and dropout layer. The one-dimensional convolution acts as the residual module for skip connections, and its output is then forwarded to the subsequent layer.

(2) GRU

GRU is advantageous for day-ahead prediction due to its simple structure and reduced number of parameters. Nevertheless, it does not possess the capability to extract specific characteristics from past data at a local level, thus necessitating the use of the TCN model for forecasting (Figure 4).

The operation expressions in the GRU unit are as follows:

$$z_t=\sigma(W_z[h_{t-1},x_t]+b_z) \tag{45}$$

$$r_t=\sigma(W_r[h_{t-1},x_t]+b_r) \tag{46}$$

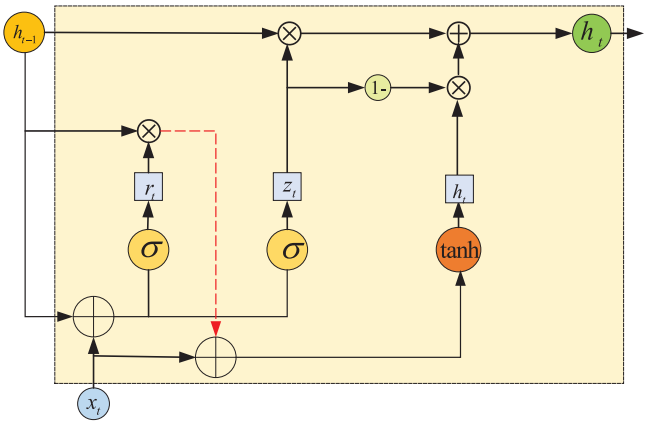

FIGURE 4 | Structure diagram of GRU.

$$\tilde{h}_t = \tanh(W_h[r_t * h_{t-1}, x_t] + b_h) \tag{47}$$

$$h_t = (1 - z_t) * h_{t-1} + z_t * \tilde{h}_t \tag{48}$$

where x_t is the input at time t, h_{t-1} is the output at time t−1, z_t is the output of the update gate, r_t is the output of the reset gate, h_t is the hidden layer state, $\tilde{h}_t$ is the candidate state and σ is the activation function.W_r, W_z and W_h are the weight matrices corresponding to the reset gate, update gate and h_t respectively;b_r, b_z and b_h are the bias matrices corresponding to the reset gate, update gate and h_t respectively.

(3) Attention mechanism

Within the framework of day-ahead prediction, this approach focuses more on important components, effectively reducing the impact of less significant or unrelated factors resulting from noise, thus improving the accuracy of the predictions. The computational formulas are expressed by Equations (49) and (50).

$$a_k = \frac{e_k}{\sum_{j=1}^{k} e_j} \tag{49}$$

$$s_k = \sum_{k=1}^{i} a_k * h_k \tag{50}$$

In Equation (49), e_k represents the dot product of the input layer at time step k and its transposed layer, a_k denotes the normalized attention weights obtained from the dot product result and s_k signifies the output of the attention mechanism layer at time step k, which weights the input layer based on the attention weights.

(4) Prediction model based on TGA

In order to enhance the accuracy and stability of forecasting under short-time step conditions, this study proposes a hybrid deep learning framework based on the TCN-GRU-attention (TGA) mechanism. This framework capitalizes on the respective advantages of convolutional and recurrent structures in time-series data modeling, while the attention mechanism enables the discrimination of salient temporal features. The overarching goal is to achieve efficient representation learning from historical data, with minimal information degradation throughout the network hierarchy.

The model architecture encompasses five core components: the input layer, TCN layer, GRU layer, attention layer and output layer. Detailed specifications are as follows:

(1) Input layer

This layer takes as input multi-source historical time-series data, including inelastic load demand, WT output and PV output, and extracts samples for training from the dataset. Let the prediction horizon be the target day, and the historical observation period be the n consecutive days prior to the target day. The historical dataset, denoted as Dataset **A**, collects three types of time-series data: WT output, PV output and inelastic load demand, with a uniform time interval of $\Delta t = 15$ min. According to the time resolution, the number of data points per day is calculated as $\frac{60}{\Delta t} \times 24 = 96$.Thus, Dataset **A** has a dimensionality of 96×n rows × 3 columns, where each column corresponds to one type of physical quantity, and each row corresponds to a 15 min time slot in the historical period. To eliminate the influence of different physical dimensions and value ranges among the three variables, column-wise independent normalization is performed on Dataset **A**. A min–max normalization method is adopted here, and the normalization formula for the kth column, where k = 1,2,3 corresponding to WT, PV, inelastic load respectively, is expressed as:

$$x_{norm}(i,k) = \frac{x(i,k) - \min(x(:,k))}{\max(x(:,k)) - \min(x(:,k))} \tag{51}$$

where $x(i,k)$ represents the ith row data of the kth column in Dataset **A**, and $x(:,k)$ denotes the full set of data in the k-th column.

Considering the independent temporal characteristics of WT, PV and inelastic load, the model adopts a single-variable input strategy: the normalized data of each column in Dataset **A** is fed into the model as an independent input sequence, rather than fusing the three variables into a multi-channel input.

(2) TCN layer

The TCN module is composed of two stacked temporal convolution blocks (TCN1 and TCN2), each incorporating causal padding, dilated convolution, batch normalization, dropout and residual connection. For the input single-variable normalized time sequence, causal padding is applied before convolution operations to ensure that the convolution output at time step t only depends on the input data at time steps ≤t. This prevents information leakage from future time steps, which is consistent with the forward temporal logic of power system data forecasting. Dilated convolutions are employed to expand the receptive field exponentially without increasing computational complexity. For the input sequence with 15 min time resolution, this mechanism enables the model to capture long-range temporal dependencies hidden in the n-day historical data, thus effectively responding to sudden fluctuations in WT/PV output caused by weather changes. Residual connections are introduced between the input and output of each convolution block to alleviate the gradient

vanishing problem during deep network training. This ensures that the gradient can be propagated efficiently through the stacked TCN layers, enhancing the stability of model convergence when processing long-sequence historical data.

(3) **GRU layer**

The sequential features extracted by the TCN blocks are fed into the GRU layer for dynamic dependency modeling, which stores and filters data information through two gating mechanisms. Aiming at the single-variable input sequence, the reset gate selectively discards irrelevant historical information, while the update gate retains critical temporal features.

The GRU layer is optimized to capture the specific nonlinear temporal features of each input variable: for WT output, it focuses on the correlation between wind speed changes and power generation; for PV output, it learns the pattern of power variation with solar irradiance during the day; for inelastic load, it identifies the periodicity of load changes caused by user behavior. This targeted learning generates optimal intermediate output values that characterize the temporal dynamics of each variable.

(4) **Attention layer**

To further strengthen the model's emphasis on influential time steps, an attention mechanism is introduced into the GRU outputs., with the implementation process tailored to the single-variable forecasting task:

The intermediate output matrix of the GRU layer is first transposed, and then the dot-product operation is performed between the transposed matrix and the original matrix to calculate the similarity score between different time steps. These scores are normalized through the softmax activation function to obtain attention weights, where higher weights are assigned to time steps with greater impact on the target day's forecasting result.

A weighted summation of the GRU intermediate outputs is performed based on the attention weights to generate a refined feature representation. This mechanism enables the model to assign greater weight to critical temporal features, thereby alleviating the attenuation of important information in long sequences.

(5) **Output layer**

The output module comprises a flattening layer, a dropout layer and a fully connected output layer with a linear activation function, and its core function is to map the refined features to the target prediction dimension:

The attention-weighted sequence features are first flattened into a one-dimensional vector to match the input dimension of the fully connected layer.

A dropout layer is then added to perform regularization, where a certain proportion of neurons are randomly deactivated during training to mitigate the overfitting risk caused by the high-dimensional historical data.

The flattened and regularized feature vector is fed into the fully connected layer with a linear activation function, which maps the feature dimension to the target output dimension corresponding to the prediction horizon. For the target day with 15 min time resolution, the output layer generates a prediction result with a dimensionality of 96 rows $\times$ 1 column, which corresponds to the 96 time slots of the target day (one data point per 15 min).

The above process (from input layer to output layer) is executed independently for each of the three columns in Dataset **A**. After completing the three rounds of single-variable forecasting, the three 96×1 column prediction results are integrated to obtain the final forecasting dataset of the target day, which covers the WT output, PV output and inelastic load demand with 15 min time resolution.

The proposed TGA model implements an end-to-end learning paradigm that co-optimizes feature extraction, temporal modelling and context-aware representation. Its modular and extensible design endows it with adaptability to varying load patterns and renewable energy penetration levels across different regions. Experimental results demonstrate that the model exhibits robust forecasting performance in complex power system environments characterized by high uncertainty and temporal variability.

4 | Case Study

In this part, a series of comparative scenarios were created using field data to assess the performance of the proposed model, and the scheduling models in the experiment were solved using the Gurobi commercial solver.

Regarding practical implementation, the proposed improved MPC-based coordinated scheduling strategy for VPPs integrating multiple resources is designed with strong engineering applicability. In terms of data support, the required input data, such as forecasting power and electricity prices, can be acquired through mature monitoring systems and market information platforms. For communication needs, the framework is compatible with industrial communication technologies commonly used in power grids, enabling real-time transmission of measurement data and scheduling instructions between the VPP control centre and distributed devices. Additionally, the bidirectional dynamic penalty mechanism is calibrated based on actual market penalty rules, and the closed-loop feedback adjustment of controllable resources complies with the operational constraints of physical devices, ensuring the executability of the scheduling strategy in engineering practice.

As an MPC-based strategy, the proposed real-time rolling optimization mechanism mandates the VPP control centre to be equipped with sufficient computing power to solve the model within the 15-min scheduling window, and even minor communication delays between the control centre and terminal distributed devices could compromise the timeliness of scheduling execution. To mitigate these issues, the current method has already incorporated a streamlined model structure, utilizing GRU instead of complex LSTM variants, to reduce computational overhead, and future research will further explore lightweight algorithm design and edge computing deployment strategies to

TABLE 1 | Parameters of TGA.

Parameters	*lr*	epoch	h_t	filters	*k*	*d*
Value	0.002	200	32	64	3	2

enhance the strategy's adaptability to low-resource hardware environments.

4.1 | Simulation Setup

The RTP and the inelastic load data used in this paper were from field data collected in the 2022 electricity market in New South Wales, Australia [43]. The primary source of data for renewable energy generation is derived from real-time power generating data obtained from a specific area. The unprocessed data was prepared and combined, resulting in separate datasets for the months of January and July. Each dataset contains the RTP, inelastic load and renewable energy production for the VPP during that specific month. The participating loads in the load side scheduling consist of private cars and taxis, with a total of 5 EVs in each category. It is presumed that the driving distance for EVs remain unaltered during the day-ahead and intra-day stage. During the day-ahead forecasting step, the deep learning system is trained using actual historical data from the VPP operation over the past four days. The output data consists of the forecasted load and generation values for the entire duration of the working day, with a time interval of 15 min. Table 1 contains the primary parameters of the deep learning algorithm. Both the day-ahead and intraday scheduling have a time span of one day and a time interval of 15 min. while Table 2 presents the performance parameters. The specifications for the VPP are provided in Table 3.

TABLE 3 | Parameters on the other resources in the VPP.

Resources in the VPP	Parameters	Value
ESS	$\text{capicity}^{\text{ESS}}$	1200 kWh
	$\text{P}^{\text{ch,ESS}}_{\text{max}}$	1000 kW
	$\text{P}^{\text{dis,ESS}}_{\text{max}}$	1000 kW
	$\text{SoC}^{\text{ESS}}_{\text{max}}$	0.8
	$\text{SoC}^{\text{ESS}}_{\text{min}}$	0.2
	$\text{SoC}^{\text{ESS}}(1)$	0.5
	y^{ESS}	0.95
Inelastic load	Capacity	3 MW
Wind power	Capacity	2 MW
Solar power	Capacity	2 MW
GT	$P^{\text{GT}}_{\text{max}}$	1500 kW
	$R^{\text{GT}}_{\text{down}}$	10 kW/min
	$R^{\text{GT}}_{\text{up}}$	−10 kW/min
Transaction power	$P^{\text{buy}}_{\text{max}}$	1800 kW
	$P^{\text{sell}}_{\text{max}}$	1200 kW
Price coefficient	λ_{ESS}	0.2 $/kWh
	α_{buy}	1
	α_{sell}	0.8
	β_{punish}	1.3
	β_{subsidy}	0.8
	λ_{GT}	0.4 $/kWh
Convergence error	ε	5%

4.2 | Day-Ahead Forecasted Data

To verify the prediction performance of the TCN-GRU-attention (TGA) model proposed in this work for the time series with different characteristics of resources in the VPP, this work selects the day-ahead PV generation, WT generation and inelastic load demand of the VPP as the prediction objects. In the meantime, to evaluate the robustness of the model, the time series of the VPP under three typical operating conditions are selected for prediction experiments, namely January 31 (typical winter scenario), July 31 (typical summer scenario) and October 31 (negative electricity price scenario). To further highlight the performance advantages of the proposed prediction model in the aforementioned VPP prediction scenarios, a comparative analysis is conducted with four other neural network models, including TCN-GRU, GRU, bidirectional gated recurrent unit with attention (Bi-GRU-attention, BGA) and bidirectional long short-term memory with TCN (TCN-Bi-LSTM, TBL).

In order to analyse the accuracy of each approach in predictions, this study selected three evaluation metrics to measure the model ability to fit the data and calculate the errors in its predictions. The metrics used include the coefficient of determination (R^2), mean absolute error (MAE) and root mean square error (RMSE). The R^2 quantifies the degree of agreement between the predicted values and the original data, where a number closer to 1 signifies a stronger alignment of the model. RMSE and MAE are utilized to quantify the extent of the prediction mistakes, where smaller values indicate superior predictive efficacy of the model. Equations (37–39) provide the evaluation formulas for these three metrics. The evaluation results of these metrics are displayed in Tables 4–6.

As given in Tables 4 and 5, it is evident that the TGA algorithm has considerably fewer prediction errors for load demand and

TABLE 2 | Parameters of EVs.

Parameters	Number	$P^{\text{ch,EV}}_{\text{max}}$	$P^{\text{dis,EV}}_{\text{max}}$	$\text{SoC}^{\text{EV}}_{\text{max}}$	$\text{SoC}^{\text{EV}}_{\text{min}}$	$\text{SoC}^{\text{EV}}(1)$	$\text{capicity}^{\text{EV}}$	y^{EV}	E^{EV}	δ_{EV}
Private EV	5	20 kW	20 kW	0.8	0.2	0.6	80kWh	0.95	0.2 kW/km	0.6$/kWh
Taxi	5	30 kW	30 kW	0.8	0.2	0.5	60 kWh	0.95	0.2 kW/km	0.6$/kWh

TABLE 4 | Prediction error of different day-ahead forecasting methods for January 31.

Method	Inelastic load			WT			PV		
	R^2	MAE (kW)	RMSE (kW)	R^2	MAE (kW)	RMSE (kW)	R^2	MAE (kW)	RMSE (kW)
TGA	0.98	33.64	42.21	0.97	42.16	65.36	0.98	57.05	105.23
TG	0.97	38.79	50.89	0.97	41.63	67.08	0.97	67.10	118.54
GRU	0.92	77.01	98.22	0.97	52.88	69.09	0.97	60.90	111.94
BGA	0.97	45.82	60.12	0.97	47.30	65.62	0.97	54.37	105.57

TABLE 5 | Prediction error of different day-ahead forecasting methods for July 31.

Method	Inelastic load			WT			PV		
	R^2	MAE (kW)	RMSE (kW)	R^2	MAE (kW)	RMSE (kW)	R^2	MAE (kW)	RMSE (kW)
TGA	0.98	38.51	44.98	0.95	70.40	96.21	0.92	94.88	164.39
TG	0.96	48.51	58.15	0.93	88.00	112.63	0.91	105.82	170.05
GRU	0.93	69.81	81.17	0.92	108.24	126.39	0.90	134.53	182.95
BGA	0.97	40.61	49.94	0.95	70.72	97.38	0.92	84.05	162.48

TABLE 6 | Prediction error of different day-ahead forecasting methods for October 31.

Method	Inelastic load			WT			PV		
	R^2	MAE (kW)	RMSE (kW)	R^2	MAE (kW)	RMSE (kW)	R^2	MAE (kW)	RMSE (kW)
TGA	0.97	36.43	49.20	0.95	70.40	96.21	0.98	57.61	86.03
TG	0.94	47.71	65.54	0.93	88.00	112.63	0.96	106.88	124.40
GRU	0.90	70.94	89.51	0.92	108.24	126.39	0.94	145.21	163.43
BGA	0.96	43.44	58.07	0.95	70.72	97.38	0.98	35.24	71.21
TBL	0.87	81.63	80.38	0.96	24.50	31.57	0.98	49.63	87.46

renewable energy generation compared to the TG and GRU algorithms. The superiority of TGA in load demand prediction for January 31st is clearly demonstrated by its 57.02% reduction in RMSE and 56.31% reduction in MAE compared to the original GRU model. While the forecast errors of TGA for renewable energy generation are comparable to those of BGA, TGA has a much lower prediction error for load demand compared to BGA. Overall, TGA demonstrates superior prediction accuracy in both datasets.

$$R^2 = 1 - \frac{\sum_{i=1}^{n}(\hat{y}_i - y_i)^2}{\sum_{i=1}^{n}(\bar{y}_i - y_i)^2} \tag{52}$$

$$\mathrm{MAE} = \frac{1}{n}\sum_{i=1}^{n}|(\hat{y}_i - y_i)| \tag{53}$$

$$\mathrm{RMSE} = \sqrt{\frac{1}{n}\sum_{i=1}^{n}(\hat{y}_i - y_i)^2} \tag{54}$$

(1) **Day-ahead inelastic load demand prediction**

To predict the day-ahead inelastic load demand of the trading day, the historical time series of the VPP's inelastic load demand in the four days prior to the trading day were input. The prediction results are illustrated in Figures 5–7, and the prediction index results are summarized in Tables 4–6. As observed from the figures, the inelastic load curve of the VPP is generally smooth with minimal nonlinear characteristics. As depicted in Figure 5a, during the daytime load peak period (10:00–18:00), the prediction results of all models basically reflect the variation trend of the actual values; however, in the rapid rise phase (12:00–16:00) and rapid decline phase (18:00–20:00), the TGA model achieves the highest consistency with the actual values, while the TG, GRU and TBL algorithms exhibit relatively larger errors. In the winter scenario (January 31st), the TBL algorithm has the worst performance among all models with MAE, RMSE and R^2, and the errors of the TG and GRU models are also significantly higher than that of the TGA. During the load valley period (4:00–8:00), all models maintain stable performance with small errors, but the TGA model still retains the optimal accuracy, while the prediction effects of the TG, GRU, BGA and TBL algorithms are slightly inferior.

Compared with the typical winter scenario, the inelastic load demand curve in the typical summer scenario (July 31st) features a larger peak-valley difference and more complex dynamic characteristics. The TGA model can more accurately capture

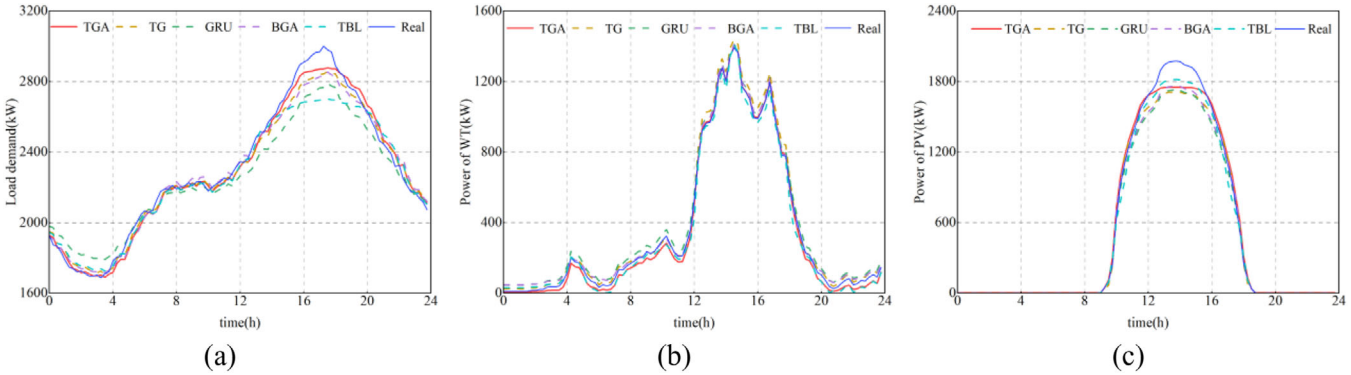

FIGURE 5 | Forecast results for January 31st (a) Inelastic load; (b) WT; (c) PV.

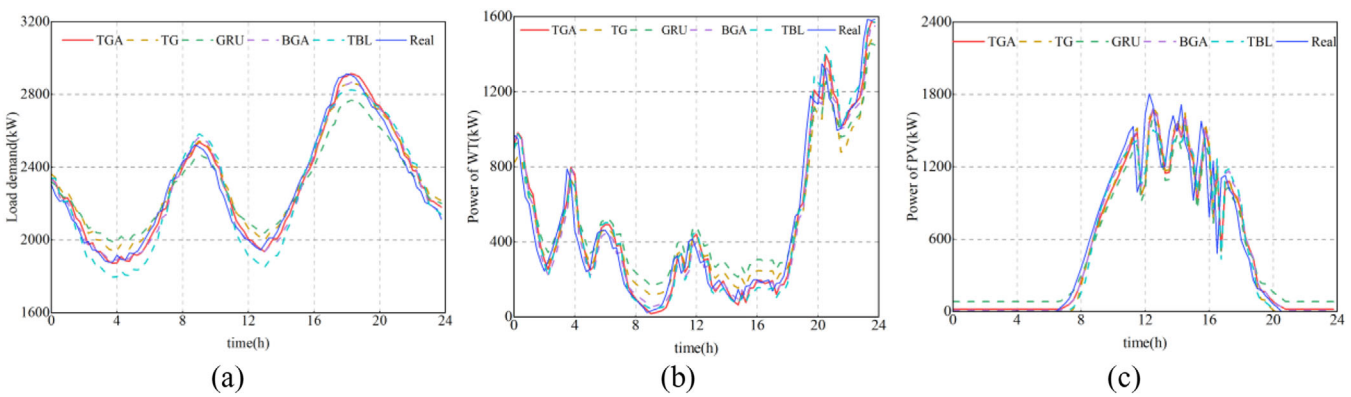

FIGURE 6 | Forecast results for July 31st (a) Inelastic load; (b) WT; (c) PV.

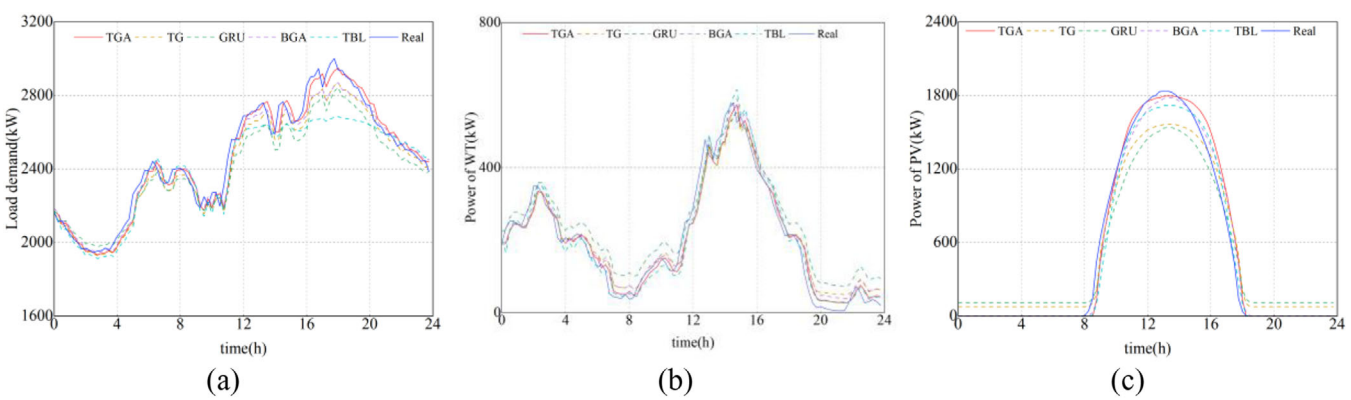

FIGURE 7 | Forecast results for October 31st (a) Inelastic load; (b) WT; (c) PV.

nonlinear changes, and its prediction performance is significantly superior to all other comparative algorithms (TG, GRU, BGA and TBL). In this scenario, the prediction accuracy of the BGA model is close to that of the TGA, while the performances of the TG, GRU and TBL algorithms are relatively poor: the TBL algorithm has an R^2 of 0.93, and its MAE and RMSE are slightly better than those of the GRU but much higher than those of the TGA and BGA, indicating limited adaptability to complex load fluctuations. As shown in Figure 7a, in the negative electricity price scenario (October 31st), load fluctuations are more significant with increased peak-valley changes and enhanced nonlinear characteristics. Under this condition, the TGA model still maintains the highest prediction accuracy during the peak period (10:00–18:00) and outperforms the TG, GRU, BGA and TBL algorithms in capturing changes in the dynamic transition phases (12:00–16:00 and 18:00–20:00).

As indicated in Tables 4–6, the TGA model exhibits optimal performance across the three scenarios, with the highest goodness of fit (R^2 up to 0.98) and the smallest errors. Specifically, in the inelastic load demand prediction for the typical winter scenario, compared with the GRU model, the RMSE of the TGA model is

reduced by 57.02% and the MAE by 56.31%. In the summer and negative electricity price scenarios, the MAE and RMSE of the TGA model also remain at the lowest levels, reduced by more than 20% and 40% compared with those of the TG, GRU and TBL algorithms, respectively. The prediction accuracy of the BGA model is close to that of the TGA but slightly inferior overall, while the performances of the TG, GRU and TBL algorithms are relatively poor.

(2) **Day-ahead WT generation prediction simulation comparison**

To predict the day-ahead WT generation of the trading day, the historical time series of the VPP's WT generation in the four days prior to the trading day were input. The prediction results are shown in Figures 5–7, and the prediction index results are presented in Tables 4–6. As can be seen from the figures, the WT generation curve of the VPP exhibits obvious nonlinear characteristics, and the correlation between WT generation and time is not significant under different scenarios. As shown in Figure 5b, all models can generally reflect the variation trend of the actual values, but during the peak period, the TGA model achieves the highest fitting degree, while the TG, GRU, BGA and TBL algorithms all have certain deviations. During the off-peak period (e.g. 4:00–8:00), all models predict stably with small errors, and the TGA model still maintains a leading position, while the accuracy of other comparative algorithms is slightly lower.

Figure 6b shows that in the typical summer scenario (July 31st), all models perform well from midnight to morning (0:00–7:00) and during the evening peak (20:00–24:00); however, in the rapid change phase (13:00–18:00), the fitting accuracy of the TGA model is significantly superior to other models. Figure 7b further indicates that in the negative electricity price scenario (October 31st), WT generation presents more complex multi-peak characteristics. Under this condition, the TGA model still exhibits excellent performance during volatile periods (e.g. 12:00–16:00), stable prediction during the valley period (4:00–8:00) and accurate capture of changes during the rapid fluctuation period (16:00–20:00). The TBL algorithm performs prominently in this scenario with the lowest MAE and RMSE among all models, but its overall stability is still inferior to that of the TGA. The BGA model ranks second, while the TG and GRU models have obvious lag and deviation.

Tables 4–6 show that the TGA model exhibits excellent high accuracy and stability in WT generation prediction. In the winter scenario, the MAE of the TGA model is 42.16 kW and the RMSE is 65.36 kW, which are 20.3% and 5.4% lower than those of the GRU model, respectively, reflecting its excellent stability in environments with small fluctuations. In the summer scenario, facing intensified WT generation fluctuations, the MAE and RMSE of the TGA model are reduced by 20.0% and 14.6% compared with the TG model, and 34.9% and 23.9% compared with the GRU model, respectively, demonstrating its strong adaptability to complex fluctuations. In the negative electricity price scenario, although the TBL algorithm shows the optimal performance in error indicators, the TGA model still maintains high accuracy, further proving its core advantage in accurately capturing dynamic changes and nonlinear characteristics. The performances of the TG, GRU and TBL algorithms are scenario-dependent, approaching advanced levels in some scenarios, but lacking sufficient consistency and stability compared with the TGA.

(3) **Day-ahead PV generation prediction simulation comparison**

To predict the day-ahead PV generation of the trading day, the historical time series of the VPP's PV generation in the four days prior to the trading day were input. The prediction results are shown in Figures 5–7, and the prediction index results are presented in Tables 4–6. The daily variation of PV generation presents a typical "bell-shaped" curve: the power gradually rises in the morning, reaches a peak at noon (12:00–14:00), then decreases, and is close to zero at night. As shown in Figure 5c, all prediction models can well capture the rising trend of power, but the prediction accuracy in the peak region is slightly insufficient. During the periods of low power (0:00–8:00 and 18:00–24:00), the prediction results of all models are relatively close to the actual values, showing stable performance. In the winter scenario (January 31st), the R^2 of the TGA model reaches 0.98, with MAE and RMSE being the optimal; the R^2 of the TBL algorithm is also 0.98, but its MAE and RMSE are slightly higher than those of the TGA, and the performances of the TG and GRU models are relatively poor.

As shown in Figure 6c, PV generation volatility is stronger in the typical summer scenario (July 31st), especially at the output peak (12:00–14:00) and rapid fluctuation period (14:00–16:00). Under this condition, the TGA and GRU models show high prediction accuracy, while the TG, BGA and TBL algorithms have obvious deviations in capturing nonlinear changes: the TBL algorithm has an R^2 of 0.91, and its MAE and RMSE are only slightly better than those of the GRU but significantly higher than those of the TGA and BGA, indicating limited adaptability to large PV output fluctuations in summer. Figure 7c shows that the PV generation curve in the negative electricity price scenario (October 31st) is more symmetrical and less volatile than that in winter. During the daytime power peak period (8:00–16:00), all models can generally reflect the actual variation trend, but the TGA model has the highest prediction accuracy in the peak region, which is significantly better than the TG, BGA and TBL algorithms. In the transition phases (e.g. 10:00–12:00 and 14:00–16:00), the TGA model can still accurately capture power changes, demonstrating excellent adaptability and stability, while the TG, GRU and TBL algorithms have certain lag and deviation.

Tables 4–6 show that the TGA model consistently maintains excellent stability and high accuracy in PV generation prediction. In the typical winter scenario, all indicators of the TGA model are superior to other models, reflecting its excellent performance in a stable PV generation environment. In the typical summer scenario, despite large fluctuations in PV generation, the MAE and RMSE of the TGA model still maintain high accuracy, showing good adaptability to large fluctuations. In the negative electricity price scenario, the MAE of the TGA model decreases to 57.61 kW and the RMSE to 86.03 kW, which are significantly lower than those of the TG and GRU models, and the overall performance is better than the BGA and TBL algorithms, further proving its accuracy and stability in complex PV generation fluctuations.

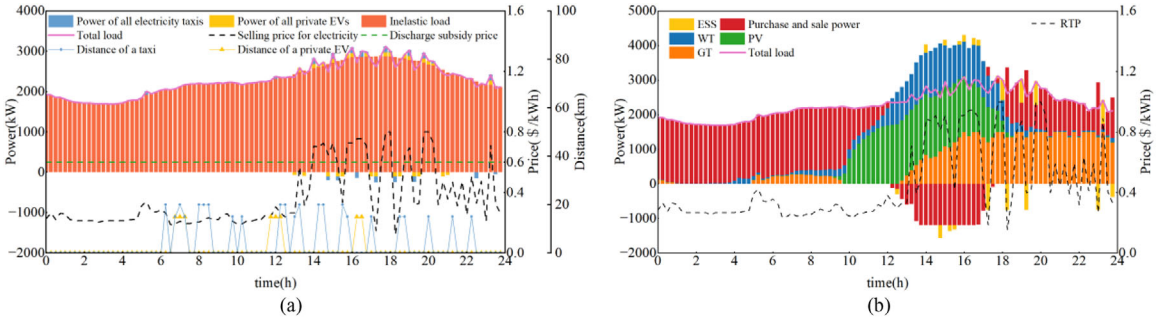

FIGURE 8 | Day-ahead scheduling for January 31 (a) load side; (b) source-storage side.

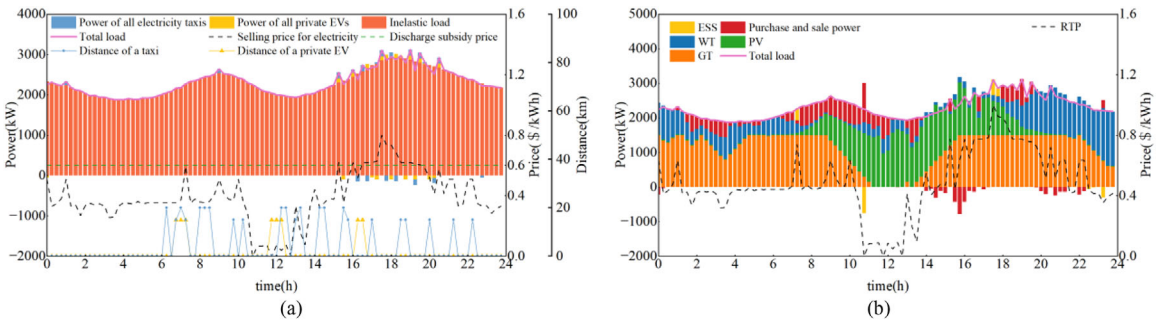

FIGURE 9 | Day-ahead scheduling for July 31st (a) load side; (b) source-storage side.

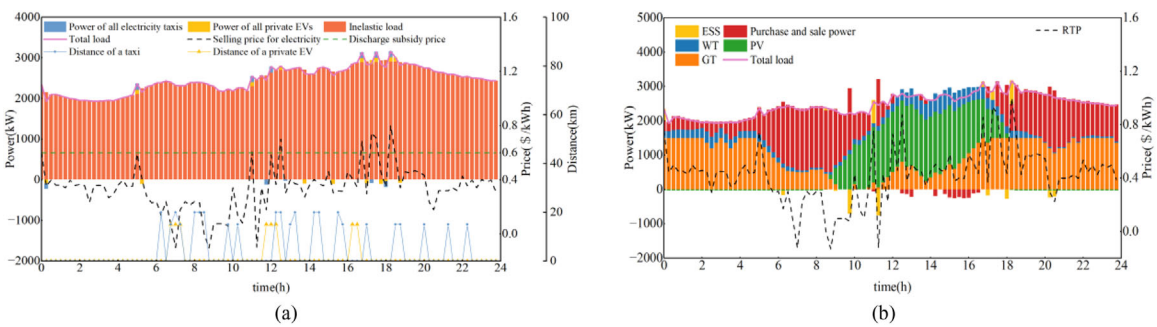

FIGURE 10 | Day-ahead scheduling for October 31st (a) load side; (b) source-storage side.

(4) **Experimental results and conclusions**

The experimental results demonstrate that the TGA model exhibits the optimal performance in the prediction of inelastic load, WT generation and PV generation. Its R^2 value can reach 0.98, and the MAE and RMSE in some scenarios are reduced by more than 20% compared with the traditional GRU model. Especially in the dynamic fluctuation phases of rapid inelastic load changes and multi-peak WT generation scenarios, the TGA model demonstrates excellent adaptability and stability.

The TGA model can effectively reduce the impact of uncertainties in renewable energy source (RES) output and inelastic load demand, providing a high-precision prediction tool for the day-ahead optimal dispatch of VPPs and improving the economy and reliability of VPPs in the electricity market.

4.3 | Day-Ahead Scheduling Plans

In order to assess the influence of various day-ahead forecasting techniques on the optimal bidding strategy of the VPP in the deregulated market, this study compares the scheduling outcomes by utilizing four forecasting methods outlined in Section 4.2. The forecast datasets and the actual dataset are inputted into the day-ahead scheduling model for analysis. The scheduling outcomes derived from the TGA method are depicted in Figures 8–10.

(1) **Day-ahead optimal dispatch results under the typical winter scenario**

The day-ahead dispatch results of the typical winter scenario are shown in Figure 8. On the load side, the charging and discharging behaviours of EVs are dynamically adjusted based on real-time electricity prices, EV travel schedules and load demands. EV

TABLE 7 | Day-ahead revenue.

Parameters		Profit	Profit from inelastic load	Profit from EVs	Cost	Costs from transactions	Costs from GT and ESS
January 31	Real	9618.79	21204.99	199.74	11785.94	5445.49	6340.45
	TGA	9420	21224.49	199.74	12264.23	5536.83	6527.4
	TG	9313.76	20973.35	199.74	11859.33	5388.38	6470.95
	GRU	9161.11	20493.25	199.74	11531.88	5143.27	6388.61
	BGA	9392.15	21088.93	199.74	11936.52	5481.66	6454.86
	TBL	9119.04	20739.14	199.74	11819.84	5367.67	6452.17
July 31	Real	9821.46	22403.79	131.2	12713.53	1645.07	11068.46
	TGA	9890.29	22455.47	131.2	12696.38	1699.35	10997.03
	TG	9400.83	22646.29	131.2	13296.66	1988.93	11307.73
	GRU	10521.73	22213.92	131.2	11823.39	791.29	11032.1
	BGA	9794.38	22387.57	131.2	12564.39	1602.47	11061.92
	TBL	9570	22248.16	131.2	12809.36	1749.64	11059.72
October 31	Real	4388.28	20417.92	130.78	16160.42	6128.59	10031.83
	TGA	4496.63	20312.01	130.78	15946.16	6038.59	9907.57
	TG	4828.61	19961.78	130.78	15263.95	5428.09	9835.86
	GRU	5048.32	19775.86	130.78	14858.32	5109.18	9749.14
	BGA	4672.94	20147.4	130.78	15605.24	5766.48	9838.76
	TBL	5008.35	19918.42	130.78	15040.85	5529.22	9511.63

Note: All monetary units in this table are US dollars.

charging and discharging activities are relatively frequent during the period from 14:00 to 20:00. When the subsidized electricity price is lower than the real-time selling price, EV discharging is scheduled to reduce load demand; when the subsidized electricity price is higher than the real-time selling price, EV charging is arranged to obtain more profits. On the source-storage side, the real-time electricity purchasing price from 0:00 to 8:00 is lower than the generation cost of GT, so electricity is purchased from the power grid to meet the load demand during this period. From 12:00 to 18:00, due to the large output of RES, the load demand can be almost fully satisfied; meanwhile, since the real-time selling price is higher than the GT generation cost, GTs maintain power generation and sell electricity to the grid. From 18:00 to 24:00, as the real-time electricity purchasing price exceeds the GT generation cost, GT power generation is prioritized to meet the load demand.

The data in Table 7 indicate that the day-ahead inelastic load revenue under TGA prediction is the closest to the real data. In terms of operating cost calculation, the day-ahead operating costs of the source-storage side under other prediction algorithms are all lower than that under TGA. Particularly under GRU prediction, the electricity purchasing and selling cost is significantly lower than the real data. This is mainly because the prediction error index adopts relative values rather than absolute values. The overall prediction error of the GRU model is relatively large, and it overestimates RES output in most time periods, leading to the underestimation of the operating cost of the source-storage side and thus falsely inflating the day-ahead profit estimation of the VPP.

(2) **Day-ahead optimal dispatch results under the typical summer scenario**

As shown in Figure 9, compared with the typical winter scenario, the peak electricity price period of the typical summer scenario is concentrated from 16:00 to 20:00, during which EV charging and discharging activities are more frequent. In the typical summer scenario, the electricity purchasing and selling power of the VPP's source-storage side participating in the electricity market is relatively small, mainly due to the following reasons: Firstly, from 0:00 to 10:00, due to the high electricity price, the VPP prefers to rely on GT power generation to meet internal demand; secondly, the time distribution of RES generation in the typical summer scenario is more uniform, and after coordination with GT, it can basically satisfy the power demand on the VPP's load side. In addition, the generation capacity of RES equipment in the typical summer scenario is limited, making it impossible to produce sufficient surplus electricity to participate in power selling activities in the electricity market.

As shown in Table 7, in the TG and TBL models, the estimated optimal bidding cost is higher than the real data, leading to the underestimation of the total profit on the load side. In contrast, the estimated optimal bidding cost in the GRU model is lower than the real data, resulting in the overestimation of the total load-side profit. By comparison, the TGA and BGA models are closer to the real data in the estimation of day-ahead bidding costs; therefore, their day-ahead dispatch results can more accurately reflect the actual situation and exhibit higher stability.

(3) **Day-ahead optimal dispatch results under the negative electricity price scenario**

As shown in Figure 10, in this scenario, negative electricity prices occur at 7:00, 9:00 and 11:00 respectively. At 5:00, 13:00 and 18:00, since the electricity selling price is higher than the discharging subsidized electricity price, the load side chooses to schedule EV charging to reduce power consumption costs. Meanwhile, due to insufficient WT output on the day, the source-storage side needs to purchase electricity on a large scale from the public power grid to maintain supply-demand balance. During the negative electricity price periods, the source-storage side achieves profitability by purchasing and storing electricity at a low price. However, this strategy also makes the electricity purchasing and selling cost of this scenario higher than that of the two previously mentioned scenarios. In addition, from 12:00 to 18:00, the real-time electricity price is higher than the GT generation cost only in a few time periods, resulting in limited power selling opportunities. Thus, the power selling volume of this scenario is lower than that of the typical winter scenario, which further affects the overall revenue.

As shown in Table 7, under the five types of prediction data, the day-ahead bidding model's estimation of the load-side profit is higher than the real data, but the estimation result based on TGA prediction data is the closest to the real data. By contrast, the deviations in profit and cost estimation based on GRU and TBL prediction data are the largest, indicating that these two models have relatively weak prediction performance under the negative electricity price scenario. Overall, the proposed model is not significantly affected by negative electricity prices under different prediction conditions and can well maintain basic control over the load-side revenue and costs. Nevertheless, the accuracy of the model still varies with different prediction methods.

Based on the optimal dispatch results of three typical scenarios presented in Figures 8–10, the environmental benefits of the proposed dispatch strategy are realized through the collaborative optimization of all adjustable resources in the VPP, which constructs a full-scenario operation mode characterized by priority accommodation of zero-emission renewable energy WT and PV, fossil energy GT as backup support, and energy storage coupled with EV load response for fluctuation suppression and adaptation to extreme electricity prices.

In winter and summer scenarios, WT and PV respectively form periodic output peaks that are precisely matched with the total load. During the corresponding periods, GT output remains consistently at a low level, only providing short-term supplementation during RES output troughs; moreover, there is no sustained peak of positive power procurement for large-scale external purchase of high-emission grid electricity.

In negative electricity price scenarios, the dispatch strategy efficiently accommodates surplus grid electricity, avoiding wasteful emissions from fossil energy caused by curtailment of surplus electricity, by guiding the off-peak response of adjustable EV charging loads and increasing energy storage charging capacity. Meanwhile, it further reduces the startup frequency and output scale of GT, this not only cuts economic costs by leveraging negative electricity prices but also enhances emission reduction effects by additionally accommodating clean electricity or replacing fossil energy-based power generation.

Overall, the peak-shaving and valley-filling of energy storage and the flexible adjustment of EV loads jointly ensure the full accommodation of renewable energy across all scenarios, significantly increasing the proportion of zero-emission energy in the VPP's power supply structure. This fundamentally reduces pollutant emissions arising from fossil energy consumption, exhibiting stable and prominent environmentally friendly characteristics under both normal operating conditions and extreme negative electricity price conditions.

As can be seen from the data in Table 7, the day-ahead optimal scheduling model and dispatch strategy proposed in this paper have improved the resource aggregation efficiency and market revenue of the VPP. However, in the unregulated electricity market, RES output fluctuations, load demand uncertainty and dynamic changes in real-time electricity prices inevitably lead to deviations between the day-ahead plan and the intraday actual operation. This not only causes the VPP to face substantial fines in the intraday market but also impairs its overall economic efficiency and operational reliability. Therefore, it is necessary to implement a more equitable penalty mechanism in the intraday calculation stage.

TABLE 8 | Other Main Parameters.

Parameters	*lr*	epoch	*dr*	filters
Value	0.001	100	0.1	64

4.4 | Intraday Scheduling Plans

This section conducts intraday dispatch based on the day-ahead dispatch scheme proposed in the previous section and adopts the three scenarios described in Section 4.3. To evaluate the economic benefits of the VPP in the intraday phase of the unregulated market under the background of source-load interaction, a comparative scheme is designed in this section: On the load side, the inelastic load maintains rolling update and prediction during the intraday phase, while the source-storage side only provides one-way response to the load-side demand without transmitting feedback signals to the load side. Under this condition, the EVs on the load side execute charging and discharging operations in accordance with the day-ahead plan during the intraday phase without further rescheduling. The parameter settings of each aggregation unit in the VPP are consistent with those in Section 4.1. In addition, the intraday imbalance penalty coefficient is set to 1.3, and the price subsidy coefficient is set to 0.8; for the specific parameter settings of the ultra-short-term prediction algorithm, refer to Table 8.

Figures 11–13 depict the scheduling results of the VPP with multiple adjustable resources and day-ahead forecasting using the TGA algorithm. On the other hand, Tables 9–11 give the income outcomes for different scenarios during the whole day.

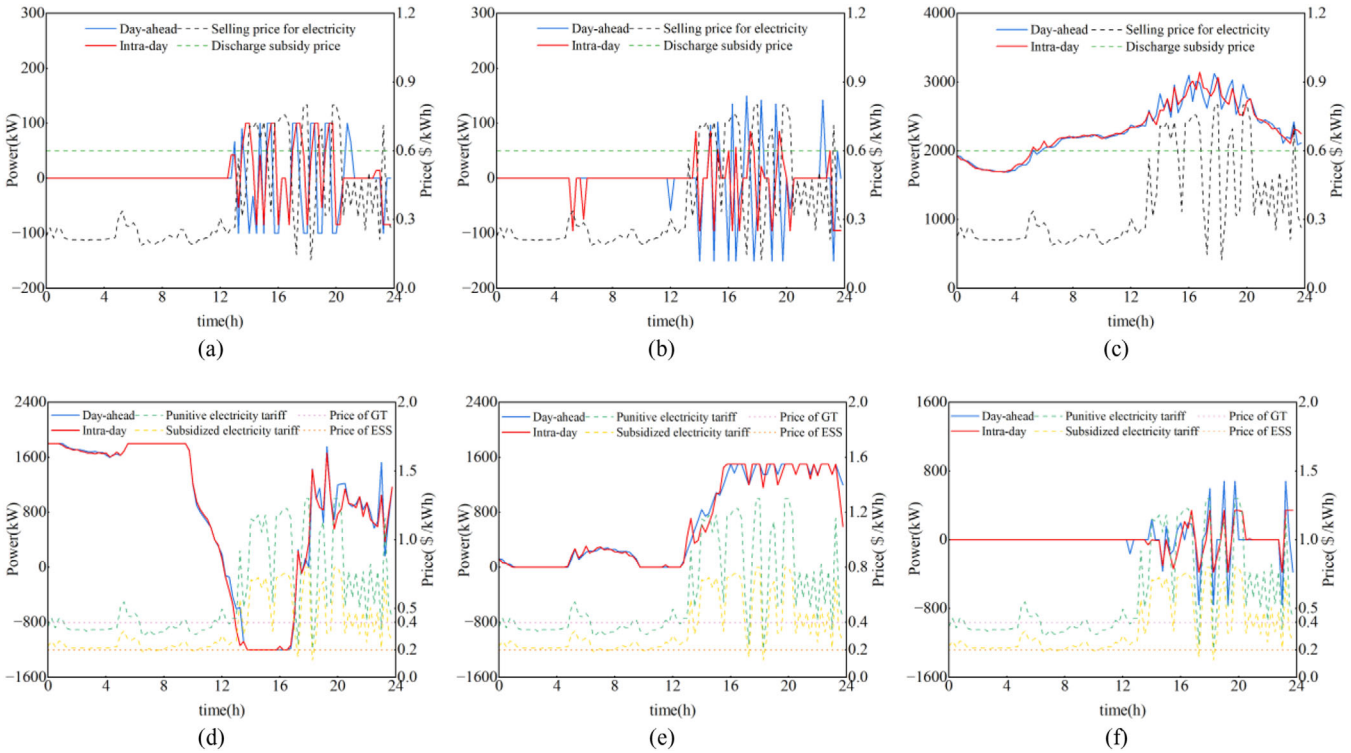

FIGURE 11 | Intraday scheduling for January 31st (a) private EVs; (b) electricity taxis; (c) total load; (d) purchase and sale power; (e) GT; (f) ESS.

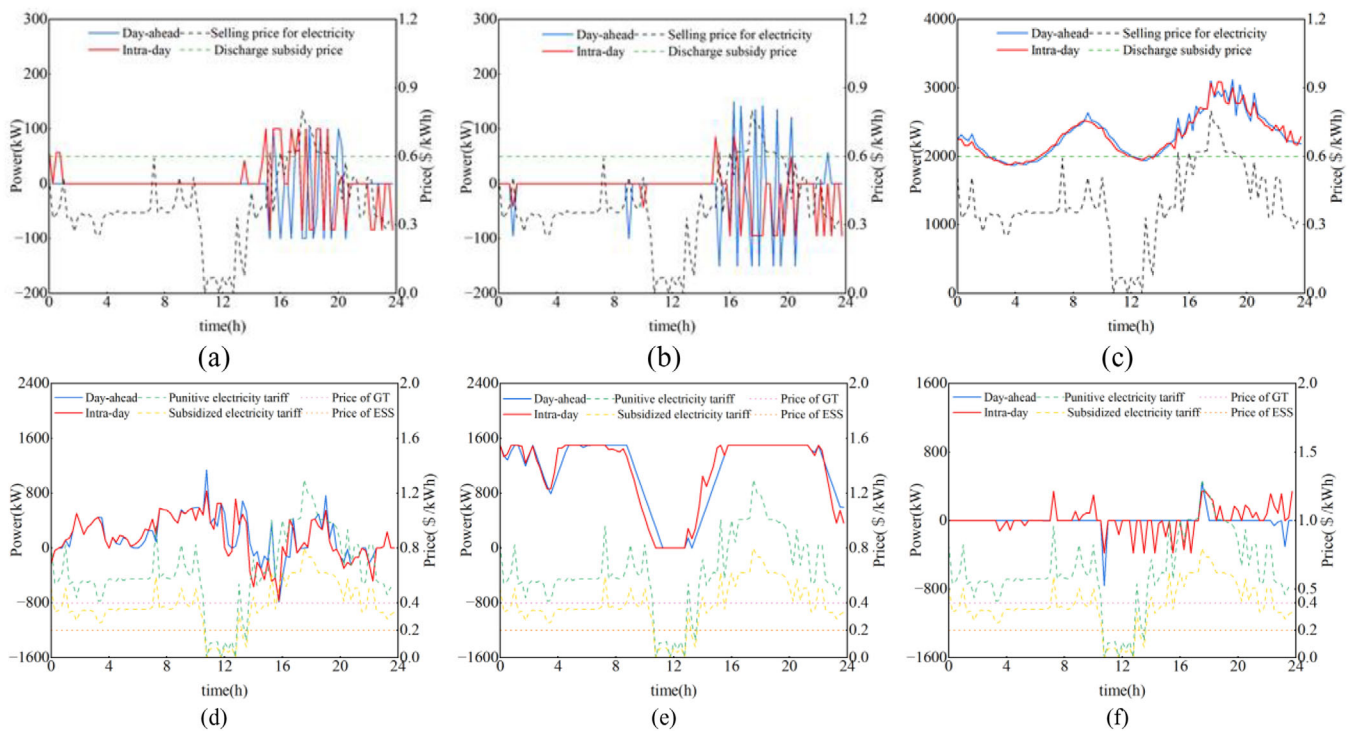

FIGURE 12 | Intraday scheduling for July 31st (a) private EVs; (b) electricity taxis; (c) total load; (d) purchase and sale power; (e) GT; (f) ESS.

(1) **Intraday optimal dispatch results under the typical winter scenario**

In the intraday revenue comparison of this scenario, the proposed scheme in this paper increases the intraday profit by 10.19% compared with the scheme using GRU day-ahead prediction without considering intraday source-load interaction.

Combined with Figure 11a,b and Table 9, it can be seen that in the intraday dispatch of the typical winter scenario, the charging and

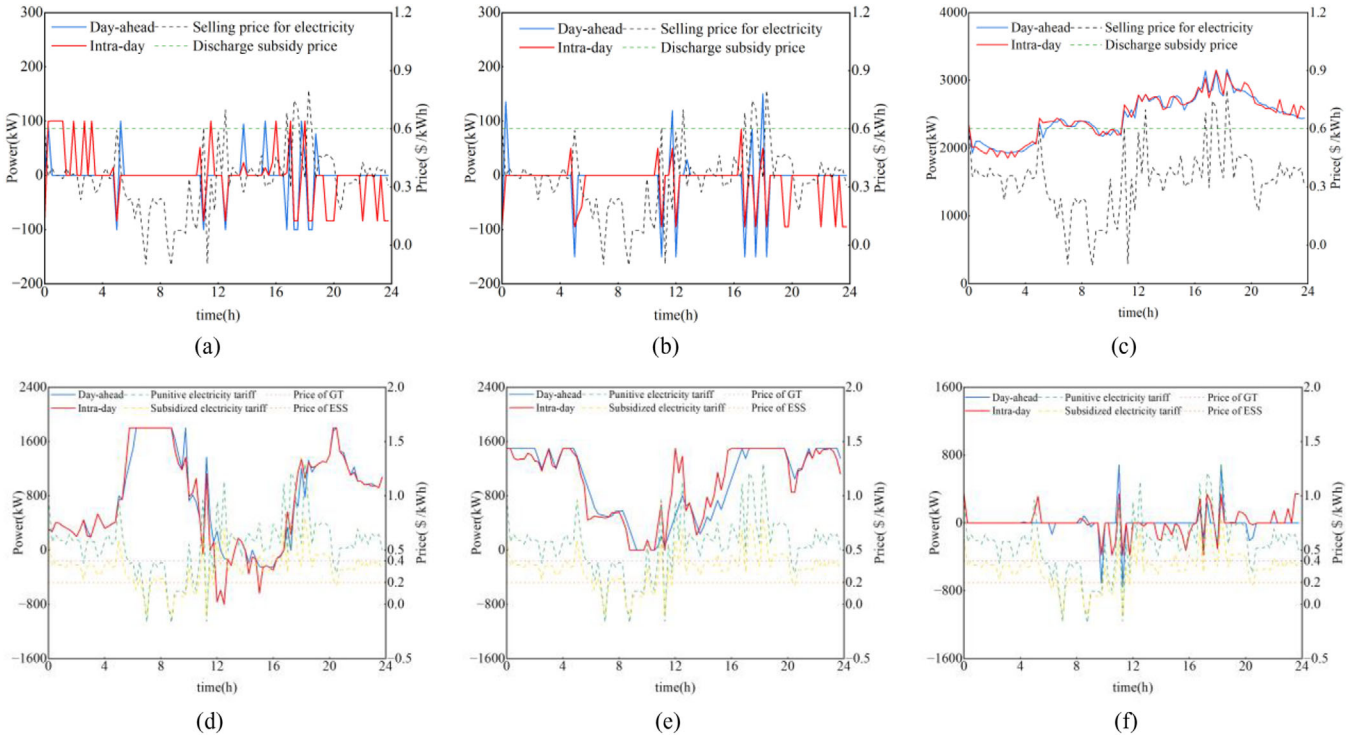

FIGURE 13 | Intraday scheduling for October 31st (a) private EVs; (b) electricity taxis; (c) total load; (d) purchase and sale power; (e) GT; (f) ESS.

TABLE 9 | Intraday revenue on January 31.

Parameters	TGA		TG		GRU		BGA	
	Case 1	Case 2	Case 1	Case 2	Case 1	Case 2	Case 1	Case 2
Profit	15,255.18	14,926.82	14,994.81	14,662.04	14,641.87	14,324.49	15,064.47	14,742.43
Profit from EVs	112.16	199.74	112.16	199.74	112.16	199.74	112.16	199.74
Cost	6061.97	6477.91	6322.34	6742.69	6675.28	7080.25	6252.68	6662.3

TABLE 10 | Intraday revenue on July 31.

Parameters	TGA		TG		GRU		BGA	
	Case 1	Case 2	Case 1	Case 2	Case 1	Case 2	Case 1	Case 2
Profit	11,425.18	11,328.97	11,765.35	11,641.55	10,513.24	10,367.8	11,354.21	11,254.06
Profit from EVs	103.06	131.2	103.06	131.2	103.06	131.2	103.06	131.2
Cost	11,081.67	11,206.02	10,741.5	10,893.44	11,993.61	12,167.19	11,152.64	11,280.93

TABLE 11 | Intraday revenue on October 31.

Parameters	TGA		TG		GRU		BGA		TBL	
	Case 1	Case 2	Case 1	Case 2	Case 1	Case 2	Case 1	Case 2	Case 1	Case 2
Profit	10,389.85	10,282.5	9737.46	9723.67	9395.1	8448.7	10,105.59	10,059.04	9821.39	9575.86
Profit from EVs	114.39	118.12	114.39	118.12	114.39	118.12	114.39	118.12	114.39	118.12
Cost	10,146.19	10,249.81	10,794.85	10,812.36	11,140.93	12,083.62	10,430.44	10,473.27	10,714.64	11,089.65

discharging power of EVs on the VPP's load side is significantly lower than the day-ahead plan. This effectively reduces the total load fluctuations on the load side, thereby lowering the intraday operating cost of the source-storage side. Although the revenue from EVs on the load side decreases, the magnitude of the reduction in operating costs is greater than that of the decrease in EV revenue, thus improving the total intraday profit of the VPP.

In addition, the intraday electricity purchasing and selling plan of the source-storage side basically achieves tracking of the day-ahead plan. From 13:00 to 20:00, the penalty electricity prices in the unregulated market fluctuate significantly. When the penalty electricity price is higher than the GT generation cost, GT output is used to compensate for intraday power fluctuations caused by day-ahead prediction errors; otherwise, the source-storage side directly bears the fines and adjusts the intraday electricity purchasing and selling plan to address deviations.

Specifically, under the GRU prediction model, the total load-side profit of the proposed scheme reaches 14,641.87 USD, an increase of 2.21% compared with 14,324.49 USD of the comparative scheme. Meanwhile, the operating cost of the source-storage side is reduced to 6675.28 USD, a decrease of 5.72% compared with 7080.25 USD of the comparative scheme. This cost-saving advantage has been verified under different prediction models such as TGA, TG and BGA. It is worth noting that the EV charging and discharging revenue of all schemes stably remains at 112.16 USD, which verifies the effectiveness of the strategy of sacrificing local interests to improve the overall operational efficiency of the system by actively suppressing EV charging and discharging power fluctuations.

(2) **Intraday optimal dispatch results under the typical summer scenario**

In the intraday dispatch of the typical summer scenario, the utilization rate of ESS is higher than the day-ahead plan. This is because from 10:00 to 19:00, the intraday penalty electricity prices in the unregulated market fluctuate significantly, leading to adjustments to the electricity purchasing and selling plan. However, GT is limited by the upper limit of its regulation capacity and cannot fully respond to power fluctuations. Therefore, ESS is required to coordinate and compensate for intraday power fluctuations through charging and discharging.

As shown in Tables 10 and 11, the total load-side profit is the lowest in the intraday dispatch under the GRU model. This is due to its large day-ahead prediction deviation, which results in significant intraday imbalanced power fluctuations and further increases the intraday penalty cost. Taking the GRU model as an example, although the total load-side profit of the proposed scheme is the lowest in summer, it is still 1.4% higher than that of the comparative scheme, which stems from a 1.43% reduction in the operating cost of the source-storage side compared with the comparative scheme. This cost reduction and efficiency improvement characteristic is more significant in the TGA model: the proposed scheme increases the load-side profit by 0.85% while reducing the operating cost of the source-storage side by 1.11%.

In addition, it is worth noting that the gap in operating costs of the proposed scheme under the BGA model narrows to 1.12%, indicating that the improvement of prediction accuracy can reduce the reliance on ESS regulation, confirming the negative correlation between the accuracy of the prediction model and the input of regulatory resources.

(3) **Intraday optimal dispatch results under the negative electricity price scenario**

Under the negative electricity price scenario, according to the analysis of power fluctuation conditions, the total load-side power fluctuates less than that in the day-ahead phase. However, the intraday charging and discharging behaviours of the two types of EVs are more frequent than those in the day-ahead phase, indicating that negative electricity prices have no significant impact on the charging and discharging behaviours of EVs. On the other hand, the GT on the source-storage side experiences large fluctuations at 12:00 in the intraday phase compared with the day-ahead phase. This is because the penalty electricity price is too high at this time, and arranging GT power generation can more effectively reduce intraday costs. In addition, at several negative electricity price time points, the intraday tie-line power fluctuations are smaller than those in the day-ahead phase, which is mainly due to the coordinated effect of ESS and GT on the source-storage side, effectively offsetting power deviations. From the perspective of total load-side profit, the performance of each model in the proposed scheme is better than that in the comparative scheme, with the GRU model achieving the largest improvement. In terms of the operating cost of the source-storage side, the cost of each model in the proposed scheme is reduced and the overall economy has achieved positive feedback.

4.5 | Economic Performance

Based on the calculation results in the above table, the optimization scheme proposed in this paper enables the VPP to obtain the maximum profit in the unregulated market and maintains a low profit volatility across different scenarios, which is superior to the comparative scheme, thus verifying the robustness of the strategy.

To more intuitively compare the revenue performance of the proposed scheme and other schemes in the day-ahead and intraday two-stage markets, this paper sets the two-stage revenue benchmark values for the typical winter scenario, typical summer scenario and negative electricity price scenario. The relative value is calculated as the actual value minus the benchmark value. The comparison of the VPP's revenue performance under different schemes in the typical winter and summer scenarios is shown in Figure 14. The results indicate that after the two-stage settlement, the advantages of the proposed scheme are mainly reflected in the following two aspects: Firstly, the TGA algorithm exhibits small prediction errors for load and RES output, resulting in a higher consistency between the day-ahead electricity purchasing and selling plan and the intraday actual situation, thereby significantly reducing the VPP's penalty cost in the intraday phase. Secondly, under the intraday source-load interaction framework, the VPP achieves a balance between EV charging and discharging revenue and operating costs, obtaining higher profits compared with the scheme that does not consider intraday source-load interaction.

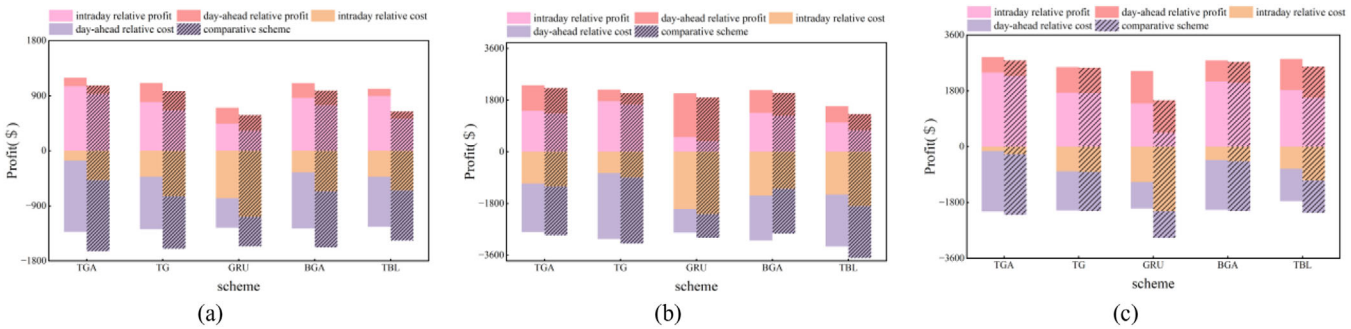

FIGURE 14 | (a) Comparison of earnings for January 31; (b) comparison of earnings for July 31; (c) comparison of earnings for October 31.

TABLE 12 | Revenue benchmark.

Profit and cost	January 31st	July 31st	October 31st
Day-ahead profit	9000	9000	4000
Intraday profit	14,000	10,000	8000
Day-ahead cost	11,000	11,000	14,000
Intraday cost	6000	10,000	10,000

However, in the typical summer scenario and negative electricity price scenario, the comparative results are less significant than those in the typical winter scenario. This is mainly because in the typical winter scenario, the electricity purchasing and selling power between the VPP and the public power grid is relatively low, leading to a small proportion of penalty costs in the VPP's total operating costs. Therefore, the impact of uncertain factors on the VPP's profit is relatively limited. Research shows that the coupling effect between the market environment and dispatch mechanism is a key factor determining the VPP's economy. The two-stage collaborative optimization model proposed in this paper provides a universal framework for multi-scenario dispatch, which can effectively improve the economic benefits of the VPP in complex market environments (Table 12).

4.6 | Comparison Results

The comparison between our proposed method and Q-learning based scheduling method of the VPP is conducted in this section to validate the effectiveness of our method [44].

The Q-learning based scheduling results of the VPP are shown in Figure 15. And the detailed comparison results are given in Table 13. Results indicate that during a typical winter day, our proposed method reduces equipment start-up and shutdown losses compared to the Q-learning method by concentrating output from gas turbines. It lowers high-cost electricity procurement expenses by adjusting power purchase and sales strategies during peak periods. Additionally, it generates extra revenue through precise arbitrage using energy storage. During a typical summer day, our approach minimized fuel waste by curtailing gas turbine output during peak PV generation, achieved arbitrage through subsequent discharge of stored surplus PV energy, and generated higher profits from combined consumption methods than from single electricity sales. In negative electricity price scenarios, our approach avoided revenue losses from selling power at low prices by storing renewable energy output, reduced fuel costs by curtailing gas turbine output and further controlled costs by decreasing peak electricity purchases.

4.7 | Comparison Results

This section conducts a sensitivity analysis for each typical intraday scenario under the TGA prediction scheme adopted by the aforementioned model, aiming to reveal the sensitivity of the economic benefits of VPPs to a core market parameter: the real-time electricity selling price. By adjusting the coefficient between electricity selling price and the real-time purchasing price (ranging from 0.7 to 1.0) in the bi-level optimization model, this study systematically explores and dissects the dynamic evolution laws of VPPs' Intraday profit, Profit from EVs, and the Intraday cost of the lower-level microgrid under three typical scenarios: January 31st, July 31st and October 31st. This analysis not only clarifies the optimal operational strategies of VPP under different market environments and seasonal conditions but also validates the inherent economic logic and game-theoretic properties of the constructed bi-level optimization model (Table 14).

(1) Sensitivity analysis under the typical winter scenario

The winter scenario fully reflects the game-theoretic attributes embedded in the proposed bi-level optimization model. As the electricity selling price coefficient increases from 0.7 to 1, the intraday profit of the virtual power plant (VPP) rises from 12159.27 to 19375.98, a cumulative growth of 59.4%, while the intraday cost decreases by 19.4% from 6401.16 to 5160.49. The results reveal a non-monotonic and intricate correlation between the profit from electric vehicles (EVs) and the electricity selling price coefficient, with the EV profit fluctuating drastically from 6.05 to a peak of 150.92 and even dropping to -6.81 at the coefficient of 0.9, exhibiting counterintuitive characteristics under specific conditions. When market conditions with high electricity selling prices exacerbate the interest conflicts between the upper-level source-storage side and lower-level adjustable resources on the load side, the upper-level source-storage side implements a rational decision-making strategy that sacrifices local EV-related gains to achieve global optimal operation. Specifically, negative profit values from EVs are deliberately generated at the coefficient of 0.9 to maximize the overall profit of the VPP system, which verifies the model's ability to balance local and global interests.

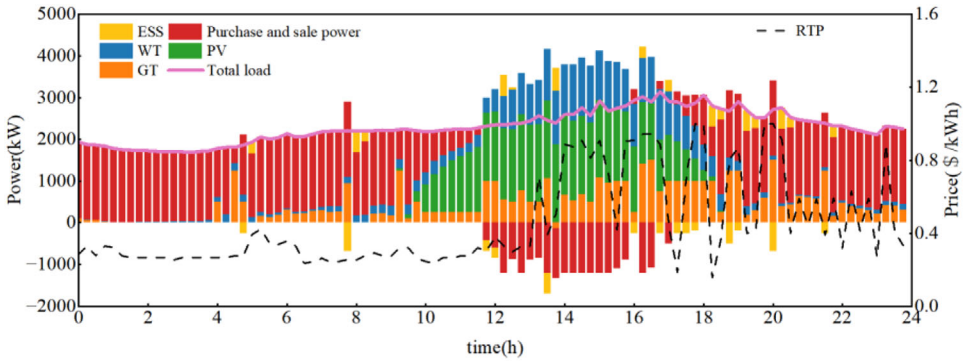

(a) scheduling results for January 31

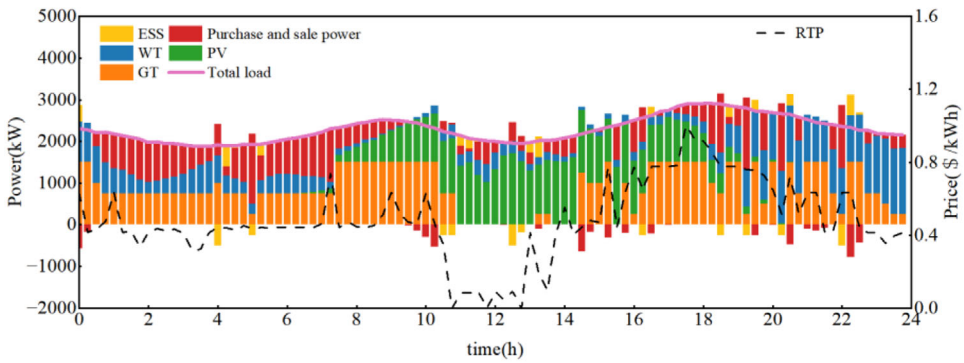

(b) scheduling results for July 31

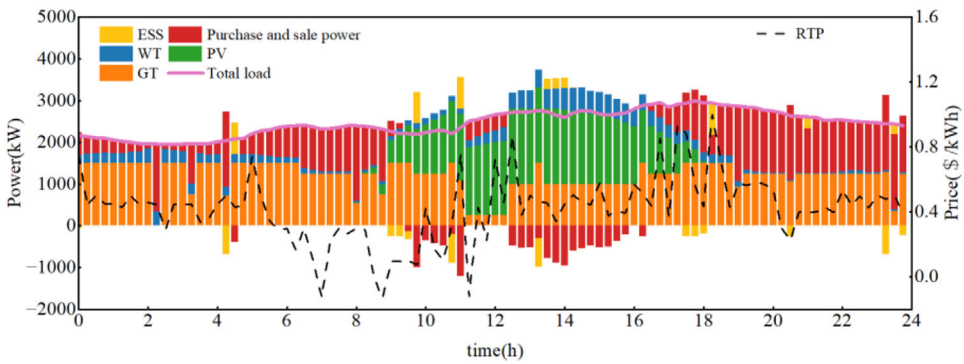

(c) scheduling results for October 31

FIGURE 15 | Q-learning based scheduling results of the VPP.

TABLE 13 | Comparison results between our proposed method and Q-learning based method of the VPP.

Typical scenarios	Economic indicators of the VPP ($)	Our proposed method	Q-learning based method	Advantages of our approach
Winter January 31	Total benefit	15,255.18	8242.92	Increased by 7012.26
	Total cost	6061.97	15,708.23	Reduced by 9646.26
Summer July 31	Total benefit	11,425.18	9236.88	Increased by 2188.3
	Total cost	11,081.67	13,924.58	Reduced by 2842.91
Negative electricity price October 31	Total benefit	10,389.85	3535.96	Increased by 6853.89
	Total cost	10,146.19	18,043.52	Reduced by 9646.26

TABLE 14 | Sensitivity analysis of electricity selling price coefficient.

Coefficient		0.7	0.8	0.85	0.9	1
January 31	Intraday profit	12,159.27	15,255.18	16,230.92	17554.29	19,375.98
	Profit from EVs	6.053	112.16	150.92	−6.81	30.23
	Intraday cost	6401.16	6061.97	5950	5294.5137	5160.49
July 31	Intraday profit	8426.64	11,425.18	12,818.69	14066.06	17,266.99
	Profit from EVs	89.08	103.06	155.13	9.0	147.21
	Intraday cost	11,265.76	11,081.67	11,140.47	11147.33	10,884.97
October 31	Intraday profit	7803.87	10,389.85	11,493.04	12895.23	15,800.16
	Profit from EVs	184.07	114.39	−57.87	−47.13	158.42
	Intraday cost	10,245.87	10,146.19	10,143	10,026.99	9880.65

(2) **Sensitivity analysis under the typical summer scenario**

The summer scenario is featured by abundant solar energy resources and high penetration of renewable energy output. As the electricity selling price coefficient increases from 0.7 to 1, the VPP intraday profit surges from 8426.64 to 17,266.99, a remarkable growth of 104.9%. In this context, the intraday operation cost of the VPP maintains a relatively high level with good stability, ranging from 10,884.97 to 11,265.76, with a maximum fluctuation of only 3.4%, and displaying a steady downward trend as the coefficient increases. Notably, the profit from EVs remains positive throughout the variation range of the coefficient, with values ranging from 9.00 to 155.13, and its fluctuation amplitude (146.13) is substantially smaller than that observed in the winter scenario (157.73). This phenomenon indicates that with sufficient renewable energy supply, the lower-level adjustable resources on the load side can not only satisfy the internal load demands of the VPP but also realize power export to the main grid. Consequently, the interest conflicts between the upper-level source-storage side and lower-level adjustable resources on the load side are significantly mitigated, and the entire system operates in a synergistic and win-win mode, rendering extreme strategic loss-making strategies unnecessary for the source-storage side.

(3) **Sensitivity analysis under the typical negative electricity price scenario**

This scenario integrates the game-theoretic characteristics of the winter scenario and the arbitrage opportunities derived from the volatile renewable energy market. As the electricity selling price coefficient increases from 0.7 to 1, the VPP intraday profit grows from 7803.87 to 15,800.16, a growth rate of 102.5%, while the intraday cost decreases slightly by 3.6% from 10,245.87 to 9880.65. The profit from EVs in this scenario presents the largest fluctuation amplitude among the three cases, with values ranging from a negative trough of −57.87 to a positive peak of 184.07, a total variation span of 241.94, far exceeding the fluctuation ranges of 157.73 in winter and 146.13 in summer. This variation pattern demonstrates that in a market environment with complex electricity price signals, the VPP exhibits highly flexible operational characteristics and opportunistic decision-making tendencies. Specifically, when the electricity price falls to a negative or extremely low level, the VPP acts as a beneficial load of the power grid to absorb surplus electricity and avoid renewable energy curtailment; when the electricity price rises and the game between the upper-level source-storage side and lower-level adjustable resources on the load side intensifies, the VPP transforms into a strategic load to balance the interest conflicts between different stakeholders; when the spread between the purchase and selling prices of electricity reaches the profitability threshold, the VPP functions as an efficient arbitrage tool to tap into the price spread benefits.

This sensitivity analysis fully validates the effectiveness of the constructed bi-level optimization model in capturing the realistic economic behaviours and intricate decision-making mechanisms of VPPs in complex market environments. It is worth noting that the charging and discharging strategy of VPPs is not dominated by the simple arbitrage logic of "buying low and selling high", but is rather the optimized outcome of dynamic game interactions between the upper-level source-storage side and lower-level adjustable resources on the load side, considering the latter's operation costs. There exists a prominent non-monotonic and scenario-dependent sensitivity relationship between the profit from EVs and the market electricity selling price coefficient: the fluctuation amplitude of EV profit in the negative electricity price scenario is 1.54 times that in winter and 1.65 times that in summer, which directly reflects the impact of scenario characteristics on the decision-making mechanism of the VPP system.

The operational strategy and profit model of VPPs are highly dependent on the characteristics of the application scenarios: in summer scenarios with abundant energy supply, the operational behaviours of VPPs show high stability and synergy, with the EV profit maintaining positivity and the intraday cost fluctuating by less than 5%; in scenarios with energy resource scarcity (winter) or complex electricity price signals (negative price scenario), the VPP operation is dominated by game-theoretic and opportunistic features and the system may even adopt strategic loss-making measures to ensure the global optimization of overall benefits.

In conclusion, this analysis provides robust empirical support for the core hypothesis of this paper, and offers solid theoretical and data-driven evidence for verifying the rationality and effectiveness of the proposed bi-level optimization model from an economic perspective.

5 | Conclusion

This paper proposes an energy-economic optimization dispatch for the VPP participating in day-ahead and intraday stages in electricity spot market. In the proposed two-stage MPC-based energy optimization scheduling, multiple adjustable resources are taken into the optimization strategies, including flexible load like adjustable EV charging load, gas turbine generation and energy storage system.

To enhance the operational efficiency of the VPP in the spot market, an MPC-based strategy and a bi-level optimization algorithm are integrated into the intraday energy management. This allows controllable resources to rapidly respond to real-time fluctuations in uncontrollable resources, while enabling EV fleets to dynamically adjust their charging and discharging schedules based on real-time feedback from resource generation. The integration of a TGA-based forecasting algorithm mitigates the adverse effects of unpredictable load demand and renewable energy output on the VPP's economic efficiency in the spot market.

The profits of the VPP in the two-stage spot market were calculated based on real-time electricity prices. Compared to other energy management schemes using different day-ahead forecasting methods and intraday optimization strategies, the proposed approach effectively manages the diverse source-load resources of the VPP, maximizing profits in the two-stage spot market. Specifically, compared to a scheme using GRU for day-ahead forecasting and single-layer MPC for intraday optimization, intraday profits increased by 10.19% and two-stage settlement profits increased by 5.06%

Future research would be focused on the evaluation of the impact of market price uncertainties. This can be addressed by enhancing the proposed scenario generation method to account for the correlation between market prices and renewable energy sources production. Additionally, for the practical implementation of the proposed architecture in real-world applications, it would be valuable to incorporate new technologies and assets into the VPP, such as hydropower plants, electric chillers, absorption chillers, ice storage systems and thermal energy storage systems.

Nomenclature

Acronyms

VPP	virtual power plant
EMS	energy management system
MPC	model predictive control
EV	electric vehicle
WT	wind turbine
ESS	energy storage system
PV	photovoltaic station
GT	gas turbine generation
RTP	real-time electricity price
SoC	state of charge

Functions

max profit	the profit function of VPP
min cost	the operating cost function of VPP

List of Variables

U_i^{EV}	the status of the EV i driving and connecting to the grid
$\mathrm{SOC}^{\mathrm{EV}}_{\mathrm{day-ahead},i}$	SOC of the EV i in the day-ahead stage
$U_i^{\mathrm{ch,EV}}/U_i^{\mathrm{dis,EV}}$	charging and discharging status of the EV i
$L^{\mathrm{im}}_{\mathrm{forcast}}/L^{\mathrm{im}}$	forecasted and actual values for non-adjustable loads
$P^{\mathrm{dis,EV}}_{\mathrm{day-ahead},i}/P^{\mathrm{ch,EV}}_{\mathrm{day-ahead},i}$	charging and discharging power of the EV i in the day-ahead stage
$L_{\mathrm{day-ahead}}/L_{\mathrm{intra-day}}$	total load of VPP in the day-ahead and intra-day stages
$P^{\mathrm{buy}}_{\mathrm{day-ahead}}/P^{\mathrm{sell}}_{\mathrm{day-ahead}}$	purchase and sale power between VPP and the public grid in the day-ahead stage
$P^{\mathrm{GT}}_{\mathrm{day-ahead}}/P^{\mathrm{GT}}_{\mathrm{intra-day}}$	the power of GT in the day-ahead and intraday stages
$P^{\mathrm{ch,ESS}}_{\mathrm{day-ahead}}/P^{\mathrm{dis,ESS}}_{\mathrm{day-ahead}}$	the power of ESS in the day-ahead and intra-day stages
$P^{\mathrm{WT}}_{\mathrm{forcast}}/P^{\mathrm{WT}}$	forecast and actual output of WT
$P^{\mathrm{PV}}_{\mathrm{forcast}}/P^{\mathrm{PV}}$	forecasted and actual output of PV
$\mathrm{SoC}^{\mathrm{ESS}}_{\mathrm{day-ahead}}$	SOC in the pre-existing phase of ESS
$P^{\mathrm{grid}}_{\mathrm{day-ahead}}/P^{\mathrm{grid}}_{\mathrm{intra-day}}$	day-ahead and intraday interconnection power between VPP and the public grid.
$P^{\mathrm{dis,EV}}_{\mathrm{intra-day,i}}/P^{\mathrm{ch,EV}}_{\mathrm{intra-day,i}}$	charging and discharging power of the EV i in the intra-day stage
$P^{\mathrm{ch,ESS}}_{\mathrm{intra-day}}/P^{\mathrm{dis,ESS}}_{\mathrm{intra-day}}$	charging and discharging power of ESS in the day-ahead and intra-day stages

List of Parameters

lr	learning rate of the neural network
k	the size of the convolutional kernel of a convolutional neural network
d	expansion coefficient of the convolutional kernel
h_t	neural network hidden layer state
y_i^{EV}	charging efficiency of the EV i
E_i^{EV}	the power consumption of the EV i per kilometre
δ_{EV}	the subsidy price coefficient for EV discharging
$\mathrm{SoC}_i^{\mathrm{EV}}(1)$	initial SoC for the EV i
$\mathrm{capicity}_i^{\mathrm{ev}}$	the capacity of the EV i
$P^{\mathrm{ch,EV}}_{\mathrm{max},i}/P^{\mathrm{dis,EV}}_{\mathrm{max},i}$	maximum charging and discharging power of the EV i

$SOC^{EV}_{max,i}/SOC^{EV}_{min,i}$	maximum and minimum SOC of the EV i
$P^{ch,ESS}_{max}/P^{dis,ESS}_{max}$	maximum charging and discharging power of ESS
$SOC^{ESS}_{max}/SOC^{ESS}_{min}$	maximum and minimum SOC of ESS
$capicity^{ESS}$	the capacity of ESS
y^{ESS}	charging efficiency of ESS
P^{GT}_{max}	maximum power of the GT
$R^{GT}_{up}/R^{GT}_{down}$	grade-up and downhill rates of GT
$P^{buy}_{max}/P^{sell}_{max}$	maximum purchase and sale power of VPP to/from the public grid
$\lambda_{GT}/\lambda_{ESS}$	price factors for GT and ESS
α_{buy}/a_{sell}	price coefficient of VPP purchasing and selling electricity to/from the public grid
$\beta_{punish}/\beta_{subsidy}$	penalty and subsidy price coefficients in the intraday imbalance market
ε	error range of the bilevel optimization

Author Contributions

Xiang Chen: conceptualization, formal analysis, methodology, software, visualization, writing – original draft, writing – review and editing. **Jinrui Tang:** conceptualization, methodology, supervision, validation, writing – original draft, writing – review and editing. **Haochen Li:** conceptualization, formal analysis, methodology, software, visualization, writing – original draft. **Changjun Xie:** supervision. **Yu Bin Xiong:** investigation, methodology. **Yang Li:** data curation, validation. **Xinhao Bian:** methodology. **Keliang Zhou:** supervision. **Leiming Suo:** methodology. **Jing Wan:** conceptualization. **Chengqing Yuan:** supervision.

Acknowledgements

This work was supported by the National Key Research and Development Program of China (No. 2021YFB2601602).

Conflicts of Interest

The authors declare no conflicts of interest.

Data Availability Statement

Data available on request from the authors.

References

1. S. Yu, X. Dong, Y. Wu, Z. Liu, C. Wang, and T. Lu, "Data-driven Robust Optimization Scheduling Model for Multi-Area Interconnected Power Grid," *International Journal of Electrical Power & Energy Systems* 173 (2025): 111418, https://doi.org/10.1016/j.ijepes.2025.111418.

2. J. Wang, Z. Cheng, J. Zhang, and D. Zhang, "Multi-Objective Optimization for Low-Carbon and Economical Scheduling in Integrated Energy System Using Hybrid Time-Scale Approaches," *Electric Power Systems Research* 253 (2026): 112526, https://doi.org/10.1016/j.epsr.2025.112526.

3. F. Mohammadi, B. Mohammadi-Ivatloo, G. B. Gharehetian, et al., "Robust Control Strategies for Microgrids: A Review," *IEEE Systems Journal* 16, no. 2 (2022): 2401–2412, https://doi.org/10.1109/JSYST.2021.3077213.

4. L. Yavuz, A. Onen, S. M. Muyeen, and I. Kamwa, "Transformation of Microgrid to Virtual Power Plant—A Comprehensive Review," *IET Generation, Transmission & Distribution* 13, no. 11 (2019): 1994–2005, https://doi.org/10.1049/iet-gtd.2018.5649.

5. S. M. Nosratabadi, R. A. Hooshmand, and E. Gholipur, "A Comprehensive Review on Microgrid and Virtual Power Plant Concepts Employed for Distributed Energy Resources Scheduling in Power Systems," *Renewable and Sustainable Energy Reviews* 67 (2017): 341–363, https://doi.org/10.1016/j.rser.2016.09.025.

6. H. M. Rouzbahani, H. Karimipour, and L. Lei, "A Review on Virtual Power Plant for Energy Management," *Sustainable Energy Technologies and Assessments* 47 (2021): 101370, https://doi.org/10.1016/j.seta.2021.101370.

7. M. Kaiss, Y. Wan, D. Gebbran, C. U. Vila, and T. Dragicevic, "Review on Virtual Power Plants/Virtual Aggregators: Concepts, Applications, Prospects and Operation Strategies," *Renewable and Sustainable Energy Reviews* 211 (2025): 115242, https://doi.org/10.1016/j.rser.2024.115242.

8. Y. Zhou, Y. Xuan, S. Chen, S. Zhou, G. Sun, and H. Zang, "Electricity-Hydrogen-Heat-Varbon Sharing Among Virtual Power Plants Considering Hydrogen Utilization for Methane and Methanol Production," 203 (2025): 153098, https://doi.org/10.1016/j.ijhydene.2025.153098.

9. J. Feng, L. Ran, Z. Wang, and M. Zhang, "Optimal Energy Scheduling of Virtual Power Plant Integrating Electric Vehicles and Energy Storage Systems Under Uncertainty," *Energy* 309 (2024): 132988, https://doi.org/10.1016/j.energy.2024.132988.

10. S. Chen, K. Zhang, N. Liu, and Y. Xie, "Unlock the Aggregated Flexibility of Electricity-Hydrogen Integrated Virtual Power Plant for Peak-Regulation," *Applied Energy* 360 (2024): 122747, https://doi.org/10.1016/j.apenergy.2024.122747.

11. M. A. Hannan, M. M. Abdolrasol, R. Mohamed, et al., "ANN-Based Binary Backtracking Search Algorithm for VPP Optimal Scheduling and Cost-Effective Evaluation," *IEEE Transactions on Industry Applications* 57, no. 6 (2021): 5603–5613, https://doi.org/10.1109/TIA.2021.3100321.

12. H. Liu, J. Qiu, and J. Zhao, "A Data-driven Scheduling Model of Virtual Power Plant Using Wasserstein Distributionally Robust Optimization," *International Journal of Electrical Power and Energy Systems* 137 (2022): 107801, https://doi.org/10.1016/j.ijepes.2021.107801.

13. Y. Li, W. Chang, and Q. Yang, "Deep Reinforcement Learning Based Hierarchical Energy Management for Virtual Power Plant With Aggregated Multiple Heterogeneous Microgrids," *Applied Energy* 382 (2025): 125333, https://doi.org/10.1016/j.apenergy.2025.125333.

14. A. Wang and D. N. Mah, "A Systematic Review on Varieties, Effectiveness and Determinants of Consumer Engagement in the Context of Electricity Market Reforms From a European-Asian Comparative Perspective," *Renewable and Sustainable Energy Reviews* 226, no. D (2026): 116430, https://doi.org/10.1016/j.rser.2025.116430.

15. X. Yang, X. Wang, F. Zhou, and L. Wang, "Multi-MG Electricity-Carbon Joint Optimization Method Considering Robust Market Clearing," *IET Generation, Transmission & Distribution* 19, no. 1 (2025): e70199, https://doi.org/10.1049/gtd2.70199.

16. Z. Zhao, Q. Ma, C. Wei, and R. Han, "Stackelberg Game Optimization Method for Virtual Power Plant and Electric Vehicle Considering Coupled Green Certificates and Spot Markets," *Expert Systems with Applications* 299, no. C (2026): 130202, https://doi.org/10.1016/j.eswa.2025.130202.

17. J. Liu, J. Peng, H. Liu, J. Deng, and X. Song, "Two-Stage Robust Optimization of a Virtual Power Plant Considering a Refined Demand Response," *Energy* 322 (2025): 135560, https://doi.org/10.1016/j.energy.2025.135560.

18. W. Jin and P. Wang, "A LSTM-Driven Stochastic Optimization Framework for Virtual Power Plant Demand Response: Integration of Multi-Tier Interruptible and Shiftable Industrial Loads," *Energy Conversion and Management: X* 27 (2025): 101144, https://doi.org/10.1016/j.ecmx.2025.101144.

19. F. Ghasemi-Olanlari, M. Moradi-Sepahvand, and T. Amraee, "Two-Stage Risk-Constrained Stochastic Optimal Bidding Strategy of Virtual Power Plant Considering Distributed Generation Outage," *IET Generation, Transmission & Distribution* 17, no. 8 (2023): 1884–1901, https://doi.org/10.1049/gtd2.12826.

20. N. Gu, J. Cui, and C. Wu, "An Auto-Tuned Robust Dispatch Strategy for Virtual Power Plants to Provide Multi-Stage Real-Time Balancing

Service," *IEEE Transactions on smart grid* 14, no. 6 (2023): 4494–4507, https://doi.org/10.1109/TSG.2023.3265398.

21. X. Yan, C. Gao, M. Song, et al., "An IGDT-Based Day-Ahead Co-Optimization of Energy and Reserve in a VPP Considering Multiple Uncertainties," *IEEE Transactions on Industry Applications* 58, no. 3 (2022): 4037–4049, https://doi.org/10.1109/TIA.2022.3152454.

22. Z. Ren, S. Li, J. Guo, D. Lin, and Y. Dong, "A Bi-Level Optimization Framework for Virtual Power Plants Integrating Electric Vehicles and Demand Response," *Sustainable Energy Technologies and Assessments* 84 (2025): 104740, https://doi.org/10.1016/j.seta.2025.104740.

23. T. Yang, X. Feng, S. Cai, Y. Niu, and H. Pen, "A Privacy-Preserving Federated Reinforcement Learning Method for Multiple Virtual Power Plants Scheduling," *IEEE Transactions on Circuits and Systems I: Regular Papers* 72, no. 4 (2025): 1939–1950, https://doi.org/10.1109/TCSI.2024.3479427.

24. Z. Bao, S. Yu, and C. Tang, "Optimal Dispatch Strategy of Virtual Power Plants With Asymmetric Information Based on Multi-Agent Deep Reinforcement Learning," *Electric Power Systems Research* 254 (2026): 112580, https://doi.org/10.1016/j.epsr.2025.112580.

25. Z. Peng and T. Heng, "Hierarchical Optimization of Virtual Power Plants via Sequential Game-Based Multi-Agent Reinforcement Learning," *Expert Systems with Applications* 310 (2026): 131263, https://doi.org/10.1016/j.eswa.2026.131263.

26. M. Khojasteh, P. Faria, F. Lezama, and Z. Vale, "A Hierarchy Model to Use Local Resources by DSO and TSO in the Balancing Market," *Energy* 267 (2023): 126461, https://doi.org/10.1016/j.energy.2022.126461.

27. Q. Li, F. Wei, Y. Zhou, et al., "A Scheduling Framework for VPP Considering Multiple Uncertainties and Flexible Resources," *Energy* 282 (2023): 128385, https://doi.org/10.1016/j.energy.2023.128385.

28. W. Zheng, L. Liu, S. Li, et al., "Smart Predict-Then-Optimize-Based Model Predictive Control for Virtual Power Plants With Battery Storage," *Journal of Energy Storage* 142 (2026): 119606, https://doi.org/10.1016/j.est.2025.119606.

29. D. Zhou, Y. Zhang, Q. Wang, and H. Ding, "How Do Uncertain Renewable Energy Induced Risks Evolve in a Two-Stage Deregulated Wholesale Power Market," *Applied Energy* 353, no. B (2024): 122140, https://doi.org/10.1016/j.apenergy.2023.122140.

30. J. H. Kim, J. S. Hwang, and Y. S. Kim, "An IGDT-WDRCC Based Optimal Bidding Strategy of VPP Aggregators in New Energy Market Considering Multiple Uncertainties," *Energy* 313 (2024): 133712, https://doi.org/10.1016/j.energy.2024.133712.

31. Y. Wang, W. Dong, and Q. Yang, "Multi-Stage Optimal Energy Management of Multi-Energy Microgrid in Deregulated Electricity Markets," *Applied Energy* 310 (2022): 118528, https://doi.org/10.1016/j.apenergy.2022.118528.

32. W. Chang, W. Dong, Y. Wang, and Q. Yang, "Two-Stage Coordinated Operation Framework for Virtual Power Plant With Aggregated Multi-Stakeholder Microgrids in a Deregulated Electricity Market," *Renewable Energy* 199 (2022): 943–956, https://doi.org/10.1016/j.renene.2022.09.037.

33. V. Babazadeh, H. Shayeghi, A. Jalili-Irani, and G. Aghajani, "Optimal Demand Response in Virtual Power Plant Using Local/Global Service Providers in Interaction With Energy Storage Systems," *Journal of Cleaner Production* 496 (2025): 145058, https://doi.org/10.1016/j.jclepro.2025.145058.

34. Z. S. M. Khozaghi, A. Seifi, and G. B. Gharehpetian, "A New Decentralized Control Structure for Generation Scheduling in a Multi-Energy Virtual Power Plant Considering Its Interactions With an Electric Vehicle Aggregator and a Demand Response Provider," *International Journal of Electrical Power & Energy Systems* 174 (2026): 111539, https://doi.org/10.1016/j.ijepes.2025.111539.

35. S. Li, H. Zhou, G. Du, S. Cao, G. Wang, and J. Duan, "Monthly Economic Scheduling Analysis of Virtual Power Plant With Electric Vehicles: Analyzing From Single-Objective to Tri-Objective Perspectives," *Energy Strategy Reviews* 61 (2025): 101848, https://doi.org/10.1016/j.esr.2025.101848.

36. J. Hu, Y. Shan, Y. Yang, et al., "Economic Model Predictive Control for Microgrid Optimization: A Review," *IEEE Transactions on Smart Grid* 15 (2024): 472–484, https://doi.org/10.1109/TSG.2023.3266253.

37. P. Han, X. Xu, Z. Yan, and Z. Tan, "Dual-Layer Model Predictive Control-Based Scheduling of Integrated Electricity-Hydrogen-Heat Microgrid," *IET Renewable Power Generation* 18, no. S1 (2024): 4638–4649, https://doi.org/10.1049/rpg2.13172.

38. Z. Zhao and W. Lin, "Short-Term Electric Load Forecasting Based on Empirical Wavelet Transform and Temporal Convolutional Network," *IET Generation, Transmission & Distribution* 18, no. 8 (2024): 1672–1683, https://doi.org/10.1049/gtd2.13151.

39. C. Yang, X. Du, D. Xu, et al., "Optimal Bidding Strategy of Renewable-Based Virtual Power Plant in the Day-Ahead Market," *International Journal of Electrical Power & Energy Systems* 144 (2023): 108557, https://doi.org/10.1016/j.ijepes.2022.108557.

40. R. Nadimi and M. Goto, "A Novel Decision Support System for Enhancing Long-Term Forecast Accuracy in Virtual Power Plants Using Bidirectional Long Short-Term Memory Networks," *Applied Energy* 382 (2025): 125273, https://doi.org/10.1016/j.apenergy.2025.125273.

41. J. Li, L. Fang, X. Wei, et al., "Short-Term Load Forecasting Facilitated by Edge Data Centres: A Coordinated Edge-Cloud Approach," *IET Smart Grid* 7, no. 6 (2024): 829–842, https://doi.org/10.1049/stg2.12181.

42. S. A. Alsamraee and S. Khanna, "A Hybrid Transformer–TCN–GRU Based Model for Thermal Load Forecasting of a Large University Campus," *Energy* 344 (2026): 140114, https://doi.org/10.1016/j.energy.2026.140114.

43. A. Prakash, A. Bruce, and I. MacGill, "The Scheduling Role of Future Pricing Information in Electricity Markets With Rising Deployments of Energy Storage: An Australian National Electricity Market Case Study," *Energy Economics* 142 (2025): 108191, https://doi.org/10.1016/j.eneco.2025.108191.

44. H. Saberi, C. Zhang, and Z. Y. Dong, "A Multi-Agent Deep Constrained Q-Learning Method for Smart Building Energy Management Under Uncertainties," *IEEE Transactions on Smart Grid* 15, no. 5 (2024): 4649–4661, https://doi.org/10.1109/TSG.2024.3386896.